



Article

Modulation of Ceramide-Induced Apoptosis in Enteric Neurons by Aryl Hydrocarbon Receptor Signaling: Unveiling a New Pathway beyond ER Stress

Mallappa Anitha ¹, Supriya M. Kumar ¹, Imhoi Koo ¹, Gary H. Perdew ¹, Shanthi Srinivasan ^{2,3} and Andrew D. Patterson ^{1,*}

¹ Department of Veterinary and Biomedical Sciences, The Pennsylvania State University, University Park, PA 16802, USA; azv2@psu.edu (M.A.); iuk41@psu.edu (I.K.); ghp2@psu.edu (G.H.P.)
² Department of Digestive Diseases, Emory University School of Medicine, Atlanta, GA 30322, USA; ssrini2@emory.edu
³ Atlanta VA Medical Center, Decatur, GA 30033, USA
* Correspondence: adp117@psu.edu

Abstract: 2,3,7,8-tetrachlorodibenzo-*p*-dioxin (TCDD), a persistent organic pollutant and a potent aryl hydrocarbon receptor (AHR) ligand, causes delayed intestinal motility and affects the survival of enteric neurons. In this study, we investigated the specific signaling pathways and molecular targets involved in TCDD-induced enteric neurotoxicity. Immortalized fetal enteric neuronal (IM-FEN) cells treated with 10 nM TCDD exhibited cytotoxicity and caspase 3/7 activation, indicating apoptosis. Increased cleaved caspase-3 expression with TCDD treatment, as assessed by immunostaining in enteric neuronal cells isolated from WT mice but not in neural crest cell-specific *Ahr* deletion mutant mice (*Wnt1Cre^{+/-}/Ahr^{b(f/f)}*), emphasized the pivotal role of AHR in this process. Importantly, the apoptosis in IM-FEN cells treated with TCDD was mediated through a ceramide-dependent pathway, independent of endoplasmic reticulum stress, as evidenced by increased ceramide synthesis and the reversal of cytotoxic effects with myriocin, a potent inhibitor of ceramide biosynthesis. We identified *Sptlc2* and *Smpd2* as potential gene targets of AHR in ceramide regulation by a chromatin immunoprecipitation (ChIP) assay in IM-FEN cells. Additionally, TCDD downregulated phosphorylated Akt and phosphorylated Ser9-GSK-3 β levels, implicating the PI3 kinase/AKT pathway in TCDD-induced neurotoxicity. Overall, this study provides important insights into the mechanisms underlying TCDD-induced enteric neurotoxicity and identifies potential targets for the development of therapeutic interventions.

Keywords: TCDD; AHR; ENS; ceramides; cytotoxicity; apoptosis



Citation: Anitha, M.; Kumar, S.M.; Koo, I.; Perdew, G.H.; Srinivasan, S.; Patterson, A.D. Modulation of Ceramide-Induced Apoptosis in Enteric Neurons by Aryl Hydrocarbon Receptor Signaling: Unveiling a New Pathway beyond ER Stress. *Int. J. Mol. Sci.* **2024**, *25*, 8581. <https://doi.org/10.3390/ijms25168581>

Academic Editor: Eugenio Vilanova

Received: 24 June 2024

Revised: 26 July 2024

Accepted: 1 August 2024

Published: 6 August 2024



Copyright: © 2024 by the authors. Licensee MDPI, Basel, Switzerland. This article is an open access article distributed under the terms and conditions of the Creative Commons Attribution (CC BY) license (<https://creativecommons.org/licenses/by/4.0/>).

1. Introduction

The interplay between environmental pollutants and biological systems has garnered considerable attention due to the pervasive nature and often long-lasting effects of these compounds. Among them, 2,3,7,8-tetrachlorodibenzo-*p*-dioxin (TCDD), a member of the dioxin family, is a persistent organic pollutant [1] known for its detrimental effects on human health and the environment due to its high lipophilicity and resistance to metabolic clearance [2]. The adverse effects of TCDD span carcinogenesis, immunotoxicity, reproductive and developmental abnormalities, and damage to the nervous system [3–8], underscoring the need for an in-depth understanding of its mechanisms of action. Of particular concern is its implications for delayed intestinal motility and enteric neuron survival, pivotal for gastrointestinal functionality [9,10].

The aryl hydrocarbon receptor (AHR), a ligand-activated transcription factor that belongs to the bHLH-PAS family [11], is a mediator of TCDD toxicity, influencing apoptosis,

cell cycle regulation, and immunomodulation [12–15]. While the role of AHR in environmental toxicology and carcinogenesis is well documented [16,17], emerging evidence suggests its involvement in apoptosis regulation [18,19], offering new perspectives on tissue homeostasis and mitigation of pathological conditions. This is of importance considering that dysregulation of apoptosis can contribute to various pathological conditions, including cancer, neurodegenerative diseases, and autoimmune disorders [20,21].

Endoplasmic reticulum (ER) stress and apoptosis have been implicated in various pathological conditions in different cell types, including neurons [22–25]. Studies have shown that AHR can induce apoptosis through ER stress in neurons [26]. Ceramides, key sphingolipid signaling molecules, are involved in various cellular processes, including cell growth, differentiation, and apoptosis [27–29]. There are three main pathways for ceramide production [30]: The de novo synthesis of ceramide occurs in the endoplasmic reticulum (ER) [31,32] and in mitochondria [33,34] with the condensation of palmitoyl-CoA and serine to form 3-ketosphinganine by serine palmitoyltransferase (SPT), and then produces ceramide by the action of ceramide synthase (CerS) and dihydroceramide desaturases (Des). The sphingomyelinase (SMase) pathway in the plasma membrane produces ceramides by the hydrolysis of sphingomyelin by the enzyme neutral sphingomyelinase (N-SMase) [35]. Ceramides can be reformed by the salvage pathway [36] that involves many enzymes, such as acid sphingomyelin phosphodiesterase (A-SMase), acid ceramidases (A-CDase), and glycosyl synthase (GCS) within the endo-lysosomal route [30]. Accumulation of ceramides has been observed in cells treated with various apoptotic agents, such as TNF- α , ionizing radiation, UV light, and chemotherapeutic agents, suggesting a ceramide-mediated role in cellular responses to these agents [37–40]. Exogenous addition of cell-permeable ceramide analogs induces apoptosis in a variety of cell lines [41–43]. Ceramide can modulate cell death by inhibiting the PI3-Kinase antiapoptotic/prosurvival pathway, which involves the regulation of Akt activity [44]. Majumder et al. have shown by genome-wide CRISPR/Cas9 screens that AHR stimulates sphingolipid levels [45]. Recent studies have demonstrated that persistent organic pollutants like TCDD, polychlorinated biphenyls (PCBs), and tetrachlorodibenzofuran (TCDF) regulate sphingolipid metabolism [46,47].

The specific role of AHR in ceramide-induced apoptosis is not well understood. Our recent studies have shown that AHR activation by TCDD affects enteric neuronal survival and delays intestinal motility in mice [9]. In this current study, we sought to extend our research by looking at the underlying molecular mechanisms of TCDD-mediated enteric neurotoxicity, the signaling pathways involved, and its molecular targets using IM-FEN cells [48]. We utilized different doses of TCDD (0.1, 1, and 10 nM) at various time points (3, 6, 12, and 24 h) to assess its effects on cell survival, ER stress markers, ceramide biosynthesis-related genes, N-SMase activity, and ceramide levels. Human exposure to TCDD typically occurs at low concentrations through contaminated food, water, and air. The levels of TCDD found in the general population are usually in the picomolar (pM) to low nanomolar (nM) range. According to the Centers for Disease Control and Prevention (CDC), background levels of TCDD in human serum typically range from 3 to 7 parts per trillion (ppt). A study by Pavuk et al. found a mean serum TCDD concentration of 5.8 ppt (~0.02 nM) in a background group of Vietnam veterans who were exposed to Agent Orange, while the mean TCDD in the low and high categories were substantially higher, 15.6 and 69.4 ppt, respectively, which corresponds to 0.05 nM and 0.2 nM [49]. Our approach helps to elucidate the potential neurotoxic effects of TCDD across different exposure levels, providing valuable insights into the risks posed by this environmental pollutant and the underlying mechanisms of its toxicity. We also examined the involvement of AHR in TCDD-induced cytotoxicity by using CH-223191, a potent and specific AHR antagonist, and primary enteric neuronal cultures from WT and neural crest cell-specific *Ahr*^{-/-} mice (*Wnt1Cre*^{+/-}/*Ahr*^{b(f/f)}). Further, we investigated the PI3K/Akt signaling pathway, which plays an important role in the regulation of enteric neuronal cell survival. Our findings suggest that AHR contributes to apoptosis in IM-FEN cells by increasing ceramide levels, which subsequently inhibits the PI3K antiapoptotic/prosurvival pathway.

2. Results

2.1. TCDD-Induced Apoptosis in IM-FEN Cells

Our laboratory has previously shown that TCDD affects IM-FEN cell survival but not proliferation [9]. This data was further supported by Western blotting showing increased expression of cleaved caspase-3, an important mediator of the apoptosis process, and cleaved PARP, which is involved in DNA repair and whose cleavage by caspases is a hallmark of apoptosis, following TCDD treatment at concentrations of 0.1, 1, and 10 nM for 24 h, indicating significant induction of apoptosis ($p < 0.0001$; Figure 1A,B). Immunofluorescence staining for TUJ1, a neuronal marker, in conjunction with TUNEL staining, which detects apoptotic cells by labeling DNA strand breaks with fluorescently labeled nucleotides, further validated these findings. IM-FEN cells treated with 10 nM TCDD for 24 h exhibited more apoptotic cells with condensed (fragmented) nuclei compared to vehicle treated cells (Figure 1C). This data underscores the critical role of TCDD in promoting neuronal apoptosis, offering insights into the mechanisms underlying TCDD-induced neurotoxicity.

2.2. AHR-Dependent TCDD-Induced Cytotoxicity and Apoptosis in IM-FEN Cells

The AHR antagonist CH-223191 preferentially blocks TCDD binding to the AHR and subsequent heterodimerization with ARNT and thus AHR-dependent mediated target gene expression [50]. To explore the involvement of AHR in TCDD-elicited cytotoxicity and apoptosis, cells were pretreated with 10 μ M CH-223191 for 1 h and then treated with Veh or 10 nM TCDD at different time points (3, 6, 12, and 24 h). Cytotoxicity was assessed by LDH release in the culture medium using the LDH-Glo Cytotoxicity Assay kit, and apoptosis was examined by assessing caspase-3/7 activity using the Caspase-Glo 3/7 Assay kit. TCDD induced a gradual increase in LDH release in the culture medium of IM-FEN cells compared to vehicle-treated cells. CH-223191 significantly mitigated the cytotoxic effects of TCDD, aligning LDH levels with those observed in vehicle-treated cells (Figure 2A), indicating that AHR was involved in the TCDD-induced effect. Additionally, caspase 3/7 activity, a marker of apoptosis, exhibited a notable increase 6 h post-TCDD exposure, diminishing at subsequent time points (12 and 24 h). CH-223191 pre-treatment effectively counteracted the rise in caspase 3/7 activity triggered by TCDD, further emphasizing the dependency of TCDD's apoptotic effects on AHR signaling (Figure 2B).

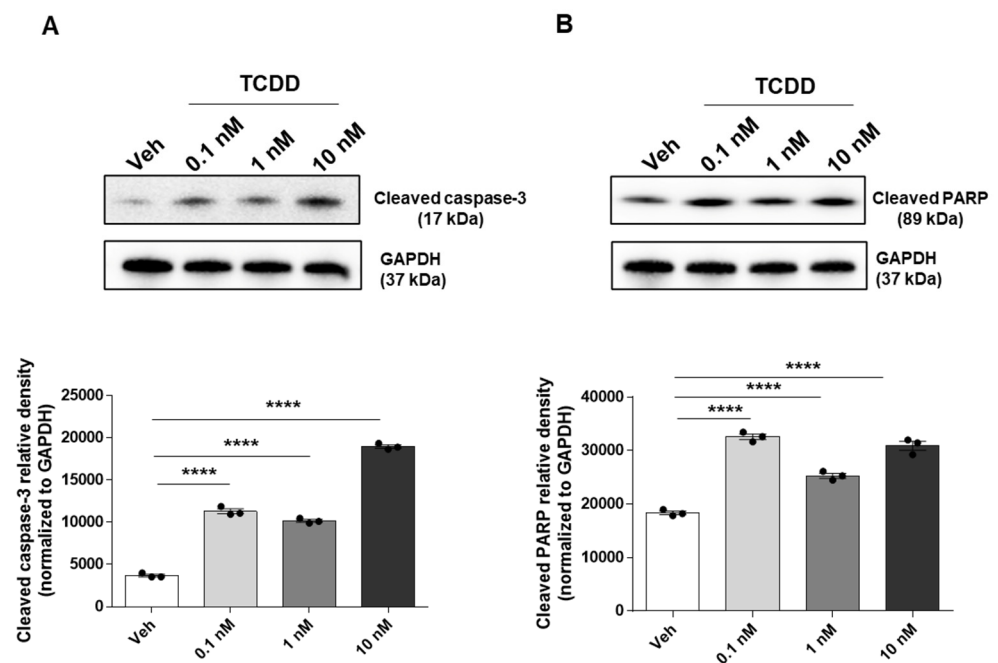


Figure 1. Cont.

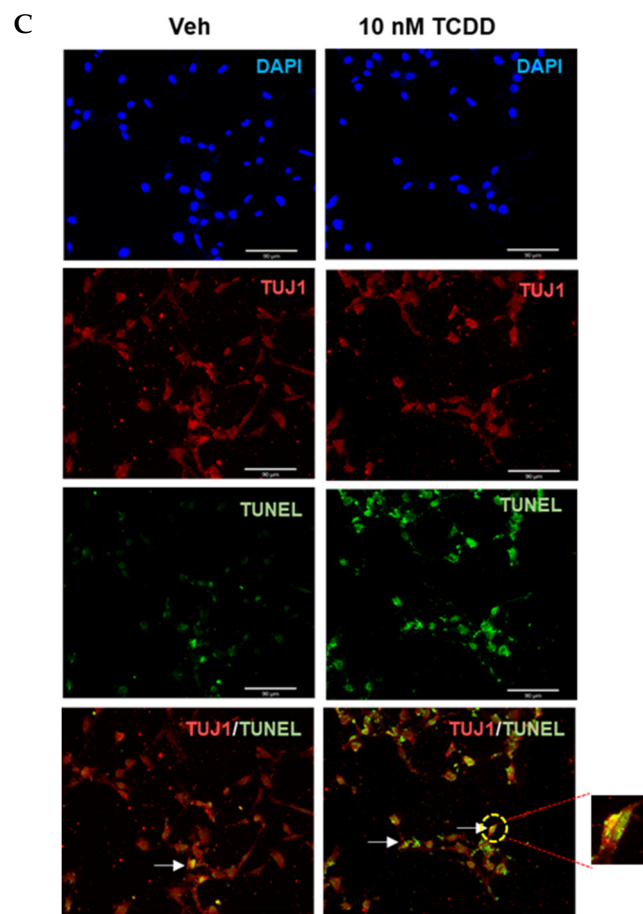


Figure 1. TCDD induces apoptosis in IM-FEN cells. Cells were treated with vehicle or various doses of TCDD (0.1, 1, and 10 nM) for 24 h. Representative images of cleaved caspase-3 and cleaved PARP Western blots are included (A,B). Results from the protein bands' density normalized to GAPDH have been included in the correspondent graphs. (C) Representative images of neuronal marker TUJ1 (red), TUNEL (green), and DAPI (blue) immunostaining in IM-FEN cells treated with vehicle and 10 nM TCDD for 24 h. Arrows point to the apoptotic cells (yellow) with condensed nuclei. Magnified image of the neuron shows the DNA fragmentation seen during apoptosis. Scale bar, 90 μm . The data represent three independent experiments. Results are mean \pm SEM, **** $p < 0.0001$.

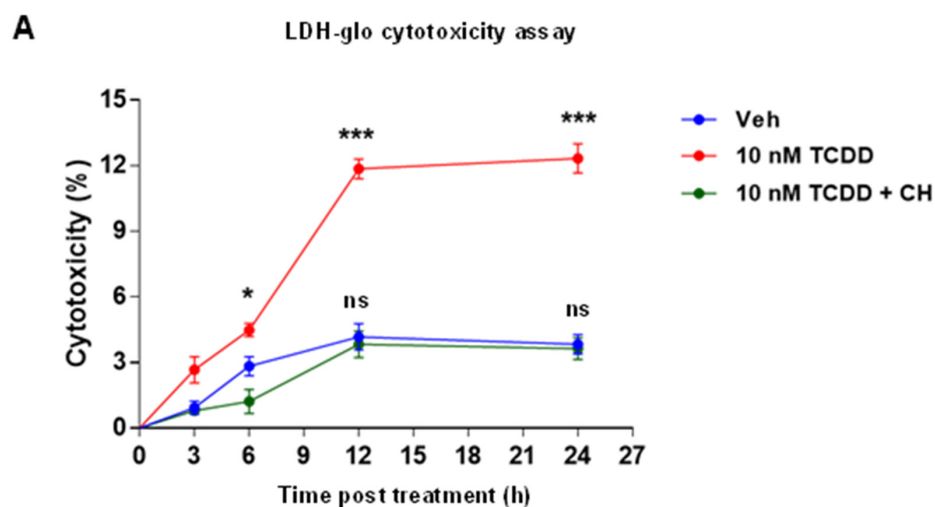


Figure 2. Cont.

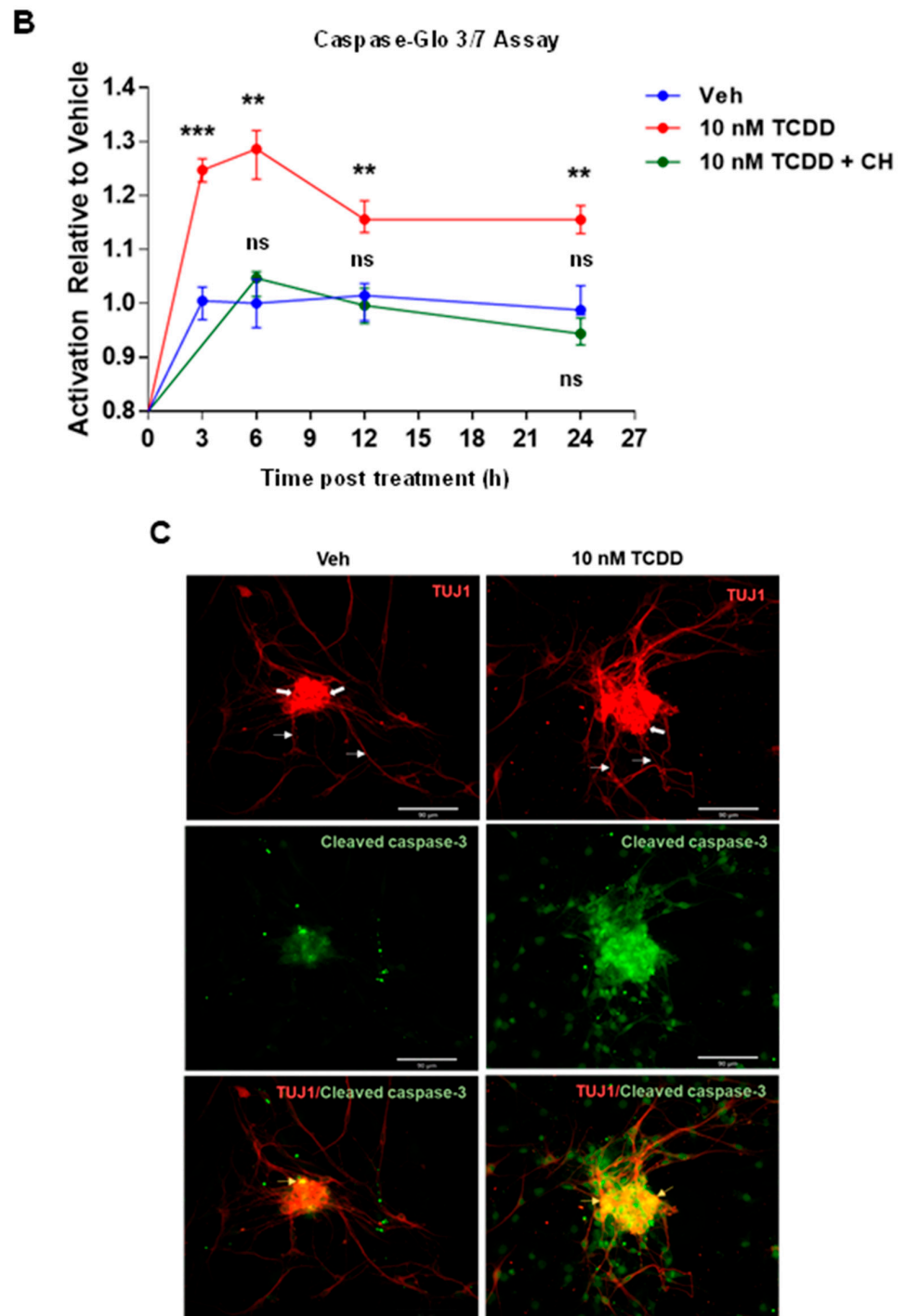


Figure 2. Cont.

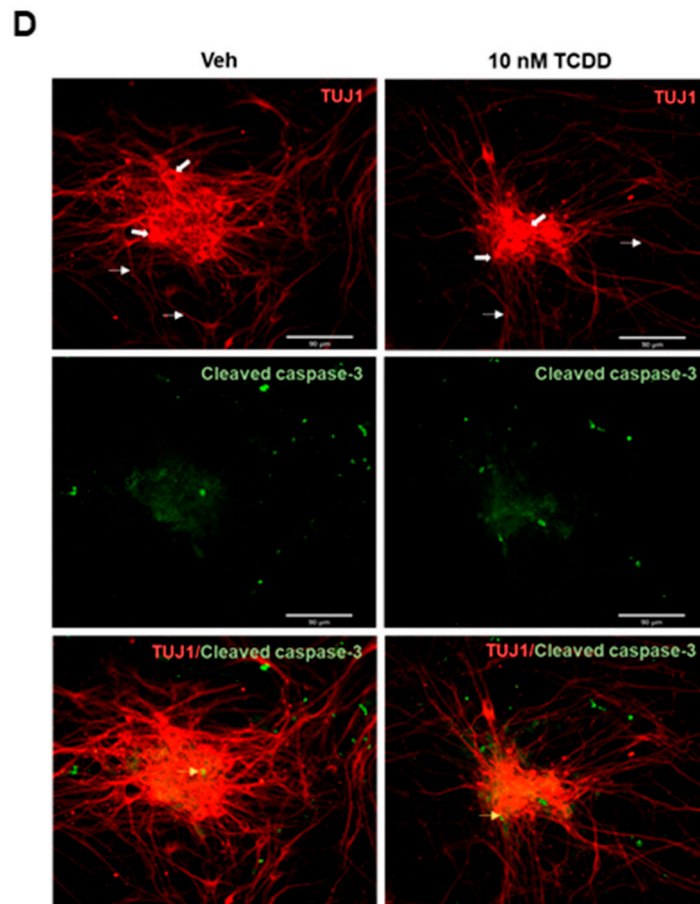


Figure 2. Cytotoxicity and apoptosis induced by TCDD are AHR-dependent. IM-FEN cells were pretreated with an AHR antagonist, CH-223191 (10 μ M), for 1 h and then treated with 10 nM TCDD at different time points (3, 6, 12, and 24 h). (A) Cytotoxicity was assessed by an LDH release assay. The percentage of cytotoxicity was calculated relative to the maximum LDH release control (10% Triton[®] X-100). (B) Cell death by apoptosis was assessed by measuring Caspase-3/7 activity 1 h after adding the Caspase-Glo-3/7 reagent. Statistical analysis of LDH cytotoxicity assay data shows significant differences between vehicle and 10 nM TCDD after 6, 12, and 24 h of treatment. Not significant (ns) differences were observed between the vehicle and 10 nM TCDD + CH-223191 experimental groups. Results from the Caspase 3/7 assay show significant differences between vehicle and 10 nM TCDD treatment at all timepoints studied, whereas n.s. differences were observed when comparing the vehicle and 10 nM TCDD + CH-223191 experimental groups. Apoptosis was assessed by TUJ1/cleaved caspase-3 immunostaining of myenteric neurons isolated from (C) *Wnt1Cre^{-/-}/Ahr^{b(f/f)}* (control) mice and (D) *Wnt1Cre^{+/-}/Ahr^{b(f/f)}* (neural crest-specific *Ahr^{-/-}*) mice treated with vehicle and 10 nM TCDD for 24 h. Representative images show TUJ1 (red) and cleaved caspase-3 (green). The white arrow points to Tuj1⁺ cell bodies, and the white arrowhead points to the axons. The yellow arrowhead points to cleaved caspase-3-positive neurons. Scale bar, 90 μ m. Results are mean \pm SEM; * $p < 0.05$; ** $p < 0.01$; *** $p < 0.001$.

Further, primary culture cells (myenteric neurons) from *Wnt1Cre^{+/-}/Ahr^{b(f/f)}* and *Wnt1Cre^{-/-}/Ahr^{b(f/f)}* mice were treated with vehicle and 10 nM TCDD for 24 h at 37 $^{\circ}$ C. Subsequently, apoptosis was examined by staining the cells with TUJ1 and cleaved caspase-3, which served as markers for neuronal cells and apoptosis, respectively. Cleaved caspase-3 expression was elevated in 10 nM TCDD-treated myenteric cells isolated from *Wnt1Cre^{-/-}/Ahr^{b(f/f)}* control mice compared to vehicle-treated cells (Figure 2C). In contrast, myenteric neurons from *Ahr^{-/-}* mice, *Wnt1Cre^{+/-}/Ahr^{b(f/f)}* mice displayed no signifi-

cant change in cleaved caspase-3 expression following TCDD treatment, highlighting the indispensable role of AHR in facilitating TCDD-induced neuronal apoptosis (Figure 2D).

2.3. TCDD-Induced Apoptosis in IM-FEN Cells Proceeds via an ER Stress-Independent Pathway

IM-FEN cells were treated with vehicle or 10 nM TCDD for 24 h. Additionally, some cells were pre-treated with the AHR antagonist CH-223191 (10 μ M) for one hour prior to a 24 h exposure to 10 nM TCDD. To benchmark ER stress, thapsigargin (300 nM, 5 h treatment) was used as a positive control. To investigate the potential role of ER stress in apoptosis induction, the expression of ER stress-associated proteins such as 78-kDa glucose-regulated protein (GRP78), inositol-requiring enzyme 1 α (IRE1 α), and the transcription factor C/EBP-homologous protein (CHOP) (Figure 3) was examined by Western blotting. The expression levels of these markers did not significantly vary across the treatment groups, corroborating the hypothesis that ER stress pathways are not implicated in the TCDD-induced apoptotic process within IM-FEN cells.

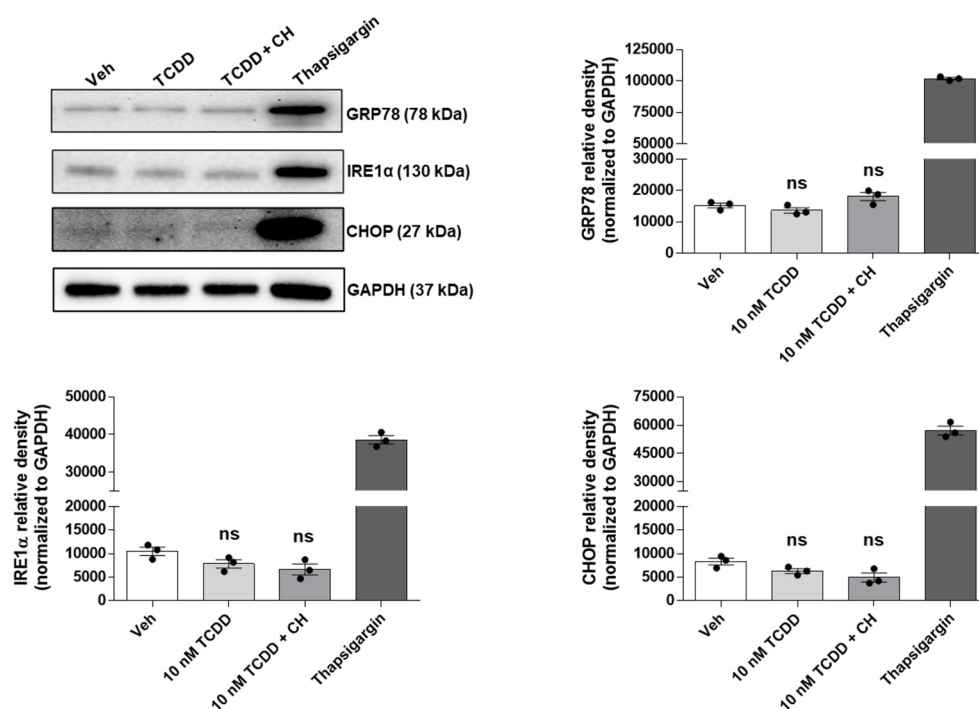


Figure 3. TCDD-induced apoptosis in IM-FEN cells is independent of ER stress. Cells were treated with Veh and 10 nM TCDD for 24 h. Some cells received pre-treatment with the AHR antagonist CH-223191 (10 μ M) for one hour before a 24 h exposure to 10 nM TCDD. Thapsigargin (300 nM, 5 h treatment) was used as a positive control for ER stress. Representative images of GRP78, IRE1 α , and CHOP Western blots are included. Results from the protein bands' density normalized to GAPDH have been included in the correspondent graphs. Results are mean \pm SEM. Not significant (ns) differences were observed between vehicle and 10 nM TCDD with or without CH-223191 experimental groups.

2.4. TCDD Regulates Ceramide Metabolism: Insights from Gene Expression, Enzymatic Activity, and Lipidomic Analyses

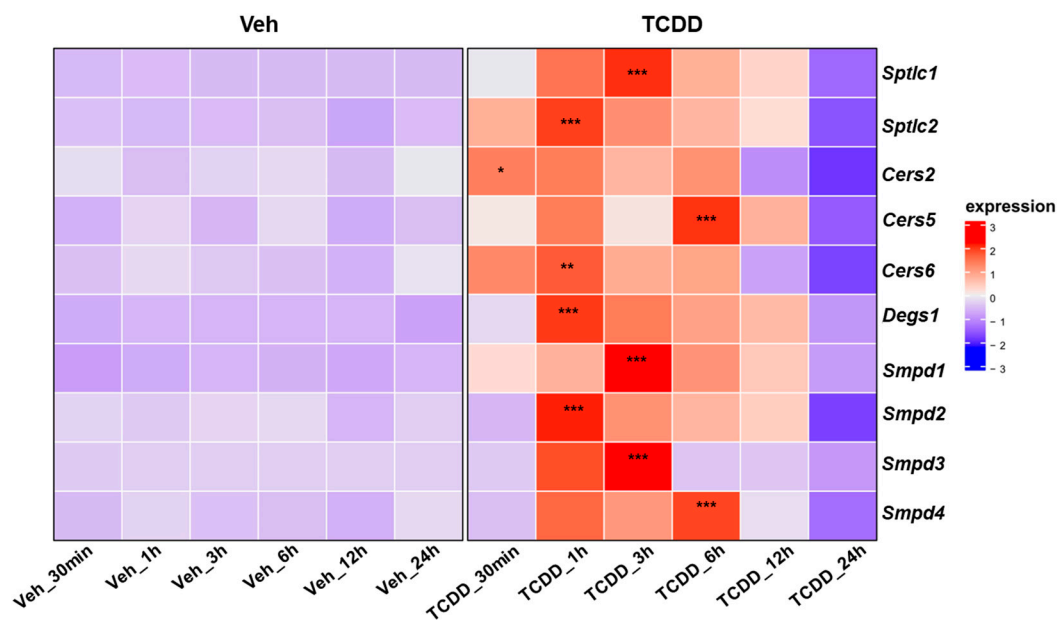
Following the exclusion of the ER stress mechanism in inducing apoptosis in IM-FEN cells, we examined the impact of AHR on the transcriptional regulation of genes encoding key enzymes involved in the ceramide synthesis pathway by qPCR using primers listed in Table 1. We observed that the expression of ceramide synthesis-related genes, including serine palmitoyltransferase long-chain base subunits (*Sptlc1*, *Sptlc2*), ceramide synthases (*Cers2*, *Cers5*, *Cers6*), dihydroceramide desaturase 1 (*Degs1*), and sphingomyelin phosphodiesterase (*Smpd1*, *Smpd2*, *Smpd3*, *Smpd4*), was significantly increased within 1 to

6 h following treatment with 10 nM TCDD. However, their expression levels decreased at 12 h and 24 h post-treatment (Figure 4A). In addition, we measured the activity of neutral sphingomyelinase (N-SMase), an enzyme involved in ceramide metabolism. We found that N-SMase activity was significantly elevated (Figure 4B, $p < 0.001$) in the IM-FEN cells following 10 nM TCDD treatment.

Table 1. Primers used for Real-time PCR.

Gene	Forward Primer (5'→3')	Reverse Primer (5'→3')
<i>B2M</i>	CATGGCTCGCTCGGTGAC	CAGTTCAGTATGTTCCGGCTTCC
<i>Sptlc1</i>	CGAGGGTTCATGGCACATT	GGTGGAGAAGCCATACGAGT
<i>Sptlc2</i>	TCACCTCCATGAAGTGCATC	CAGGCGTCTCTGAAATACC
<i>Cers2</i>	AAGTGGGAAACGGAGTAGCG	ACAGGCAGCCATAGTCGTTC
<i>Cers5</i>	CTTCTCCGTGAGGATGCTGT	GTGTCATTGGGTTCCACCTT
<i>Cers6</i>	AAGCCAATGGACCACAAACT	TGCTTGGAGAGCCCTTCTAAT
<i>Degs1</i>	AATGGGTCTACACGGACCAG	TGGTCAGGTTTCATCAAGGAC
<i>Smpd1</i>	GTTACCAGCTGATGCCCTTC	AGCAGGATCTGTGGAGTTG
<i>Smpd2</i>	GACATCCCCTACCTGAGCAA	CCAGGAGAGCCAGATCAAAG
<i>Smpd3</i>	CCTGACCAGTGCCATTCTTT	AGAAACCCGGTCCCTCGTACT
<i>Smpd4</i>	ACCTGGCCCTCAATCCATTG	ATAGGCACAGTCCGAAGTACG

A



B

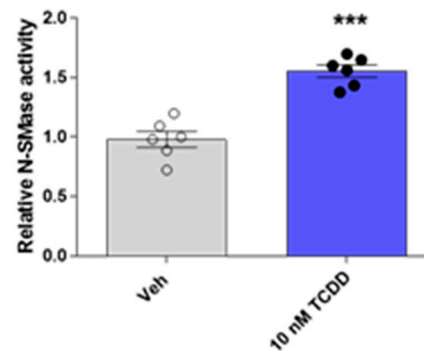
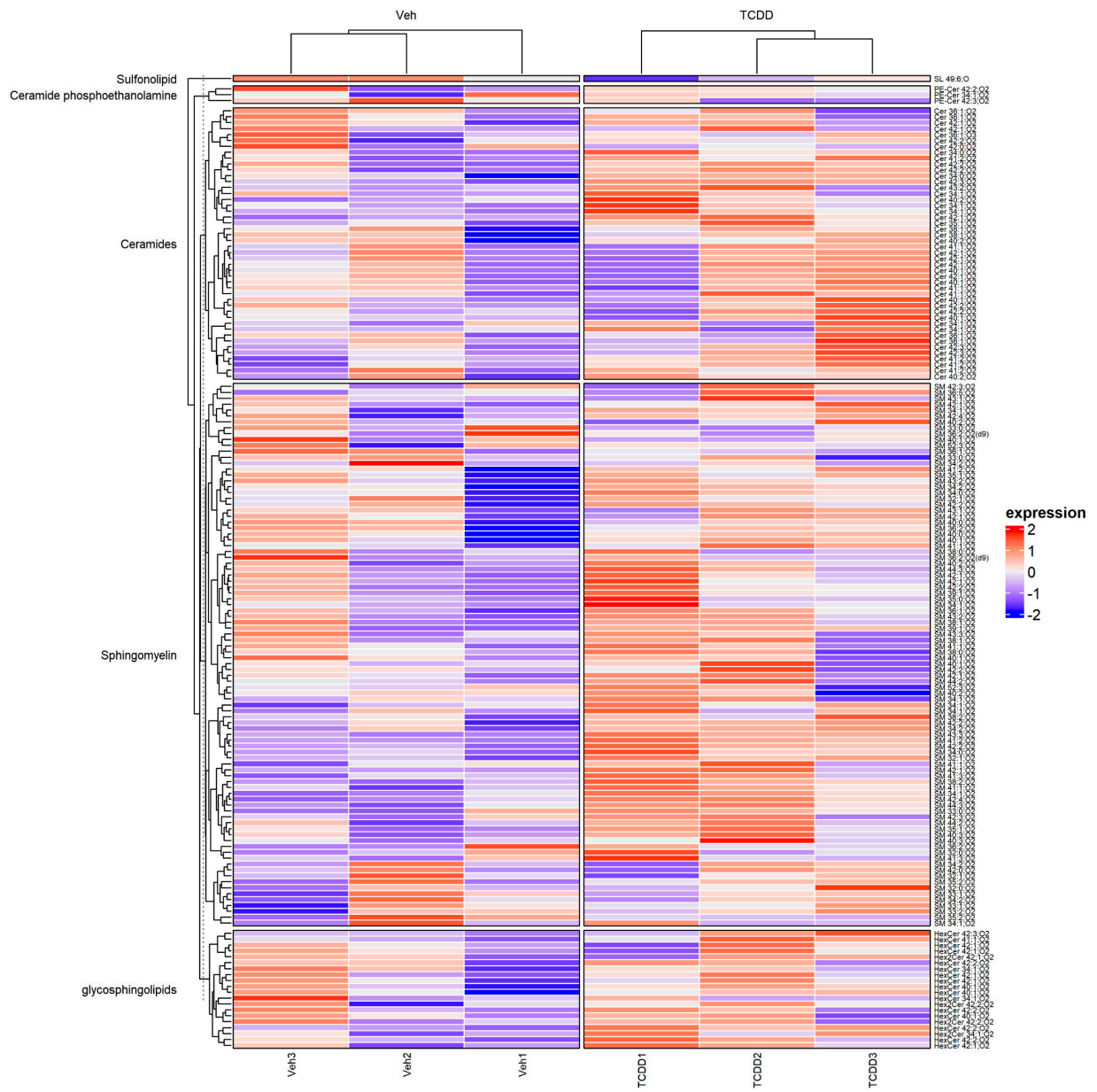


Figure 4. Cont.

C



D

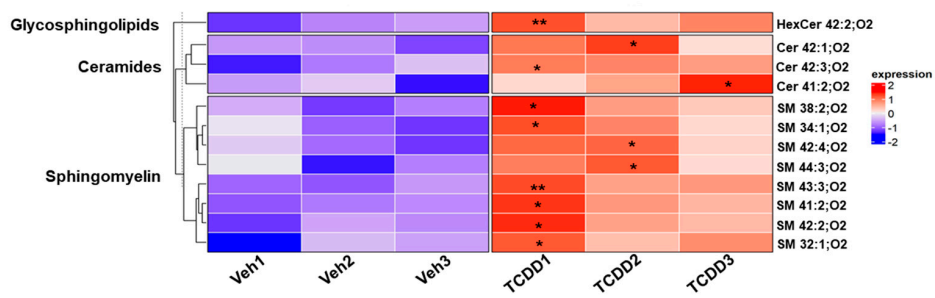


Figure 4. Cont.

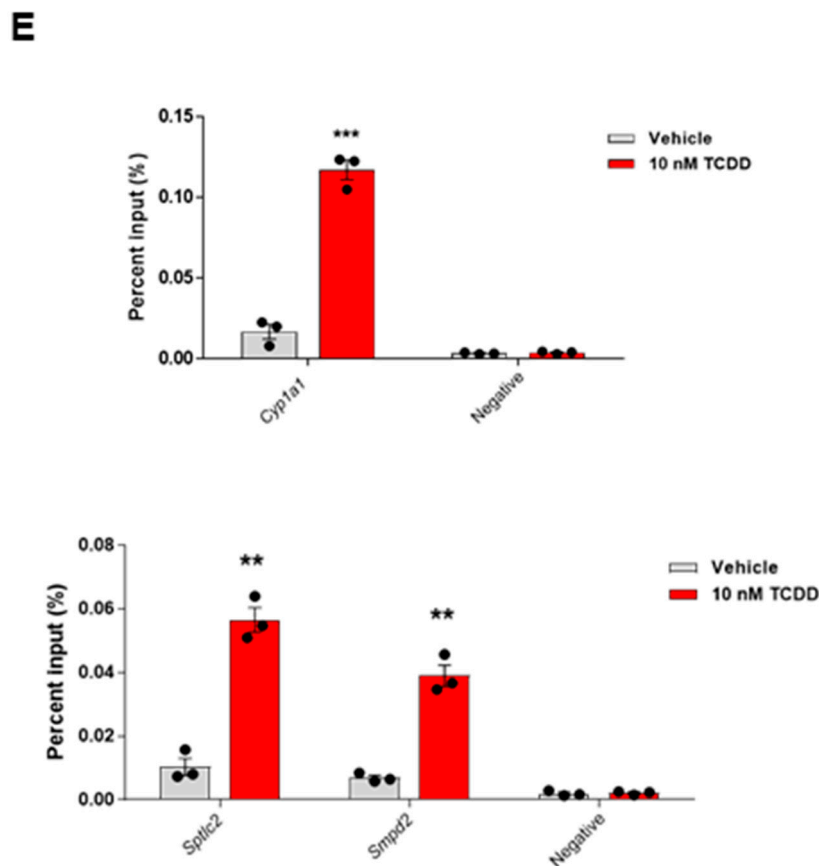


Figure 4. Regulation of ceramide biosynthesis and sphingolipid metabolism by TCDD in IM-FEN cells. Quantitative PCR (qPCR), neutral sphingomyelinase (N-SMase) activity assays, lipidomics, and chromatin immunoprecipitation (ChIP) assays to elucidate the effects of TCDD treatment on ceramide metabolism and gene regulation. (A) Heat map visualization shows the normalized expression levels of key genes involved in ceramide biosynthesis (*Sptlc1*, *Sptlc2*, *Cers2*, *Cser5*, *Cers6*, *Degs1*, *Smpd1*, *Smpd2*, *Smpd3*, and *Smpd4*) in IM-FEN cells treated with vehicle or 10 nM TCDD over various time points (30 min, 1, 3, 6, 12, and 24 h), with upregulated genes in red and downregulated genes in blue. Columns represent the timepoint, and rows represent individual genes. (B) N-SMase activity of vehicle and 10 nM TCDD-treated IM-FEN cells for 24 h. (C) Lipidomics analysis presented through a heatmap, illustrating the log₂ mean-centered normalized data of sphingolipids in vehicle and 10 nM TCDD-treated IM-FEN cells, with tiles colored red for high abundance and blue for low abundance. (D) Statistically significant changes in sphingolipids, sorted into categories, are highlighted to show the alterations in ceramide, sphingomyelin, and hexosylceramide levels. log₂ mean-centered data were imported into R, and the Complex Heatmap package was used to create the heatmap. (E,F) IM-FEN cells were treated with vehicle and 10 nM TCDD for 1 h. (E) ChIP-qPCR result for *Cyp11a1* gene promoter. (F) ChIP-qPCR results for *Sptlc2* and *Smpd2* gene promoters that were quantified by normalization with the corresponding input signal. Results are mean \pm SEM, * $p < 0.05$; ** $p < 0.01$; *** $p < 0.001$.

To delve deeper into the effects of TCDD on the ceramide synthesis pathway, the sphingolipid metabolism of IM-FEN cells treated with vehicle and 10 nM TCDD for 3 h was analyzed via lipidomics. This analysis, represented through heatmaps, uncovered significant differences in the levels of various sphingolipids, including ceramide, sphingomyelin, and hexosylceramide, in IM-FEN cells treated with TCDD compared to vehicle-treated cells (Figure 4C,D). Total ion chromatogram (TIC)-based normalization values were applied to the heatmap.

To further investigate the potential ceramide gene targets of AHR, genomic DNA fragments bound by AHR were analyzed by a Chromatin Immunoprecipitation (ChIP)

assay. For the ChIP assay, IM-FEN cells were treated with vehicle and 10 nM TCDD for 1 h. Immunoprecipitated DNA was amplified and quantified by qPCR with primers for *Cyp1a1* (positive control), *Sptlc2*, and *Smpd2* gene promoters containing known and suspected DREs (Table 2). The ChIP-qPCR showed a significant increase in the percentage of *Cyp1a1* in AHR-recognized genomic DNA fragments (Figure 4E, $p < 0.001$) in the TCDD treated cells. The percentage of *Sptlc2* and *Smpd2* in AHR-recognized genomic DNA fragments increased significantly after TCDD treatment (Figure 4F). These results suggest that AHR directly binds to the promoters of *Sptlc2* and *Smpd2*, indicating their regulatory involvement in ceramide synthesis pathway modulation. This direct targeting by AHR underscores the intricate regulation of ceramide metabolism following TCDD exposure.

Table 2. Primer sequences for ChIP-PCR (qPCR).

Gene	Abbreviation	Sequence
Cytochrome P450, family 1, subfamily A, polypeptide 1	<i>Cyp1a1</i>	CAGAGGATGGAGCAGGCTTA AGGATCCACGCGAGACAG
Serine palmitoyltransferase, long chain base subunit 2	<i>Sptlc2</i>	ACCTCTCCGAAACCGGAAAT GCGAGCCCCGTCTTCTC
Sphingomyelin phosphodiesterase 2	<i>Smpd2</i>	AGAGAGGGTTGTGTGTGTGC GATGATGAAGTTGGCAGAGC
Negative control		CAGCAGCTCTTTGTGCTGAC TCCATCTGTGCAGCCTGTAG

The results collectively demonstrate that TCDD-induced activation of AHR leads to the upregulation of ceramide synthesis-related genes and an increase in N-SMase activity. These findings highlight a potential mechanistic link between AHR activation and ceramide metabolism in IM-FEN cells, suggesting a pivotal role of AHR in modulating ceramide metabolism.

2.5. Induction of Cytotoxicity and Apoptosis by Short-Chain Ceramides in IM-FEN Cells

Ceramides have been found to induce cytotoxicity by triggering apoptosis [44,51]. In our study, we investigated the impact of TCDD treatment on ceramide synthesis and its potential role in apoptosis in IM-FEN cells. We specifically examined the effects of short-chain ceramides (C_2 -ceramide and C_6 -ceramide) on cell viability and apoptosis, as these forms of ceramides can easily penetrate the cell membrane compared to natural long-chain ceramides [42]. To assess cytotoxicity and apoptosis induction, we utilized both cytotoxicity assays measuring lactate dehydrogenase (LDH) release and caspase-3/7 activity assays. IM-FEN cells were exposed to various treatments: vehicle, 25 μ M C_2 - and C_6 -ceramides, as well as inactive analogs called C_2 - and C_6 - dihydroceramides (DHC) (25 μ M), which served as negative controls. We monitored the cells at different time points: 30 min, and 1, 3, 6, 12, and 24 h. The LDH release assay indicated an increase in cytotoxicity following treatment with C_2 -ceramide and C_6 -ceramide, marked by elevated LDH levels in the medium, suggesting compromised cell membrane integrity. This effect was most pronounced within the first 6 h post-treatment and showed a decline over time, highlighting the temporal dynamics of ceramide-induced cytotoxicity (Figure 5A).

Furthermore, we examined caspase 3/7 activity, which serves as an indicator of apoptosis. With C_2 -ceramide treatment, we observed higher caspase 3/7 activity at 3 and 6 h, while C_6 -ceramide treatment resulted in increased caspase 3/7 activity at 6 and 12 h (Figure 5B). These findings suggest that the timing and magnitude of caspase activation may vary depending on the specific ceramide treatment. In contrast, treatments with C_2 - and C_6 -dihydroceramides (DHC), inactive analogs of ceramides, did not elicit similar cytotoxic or apoptotic responses, underscoring the specificity of ceramide action. The percentage of cytotoxicity and caspase activity for treatments with C_2 - and C_6 -ceramide reaching zero starting at 12 h indicates that maximum cytotoxicity was likely achieved,

leading to the death of all cells. This suggests that any remaining cells are either resistant or that the assay reached its maximal detection limit, thus showing no further increase in measured activity. The zero value indicates that additional ceramide treatment does not further impact cell viability or caspase activity, likely due to the saturation of the ceramide effect within the experimental conditions.

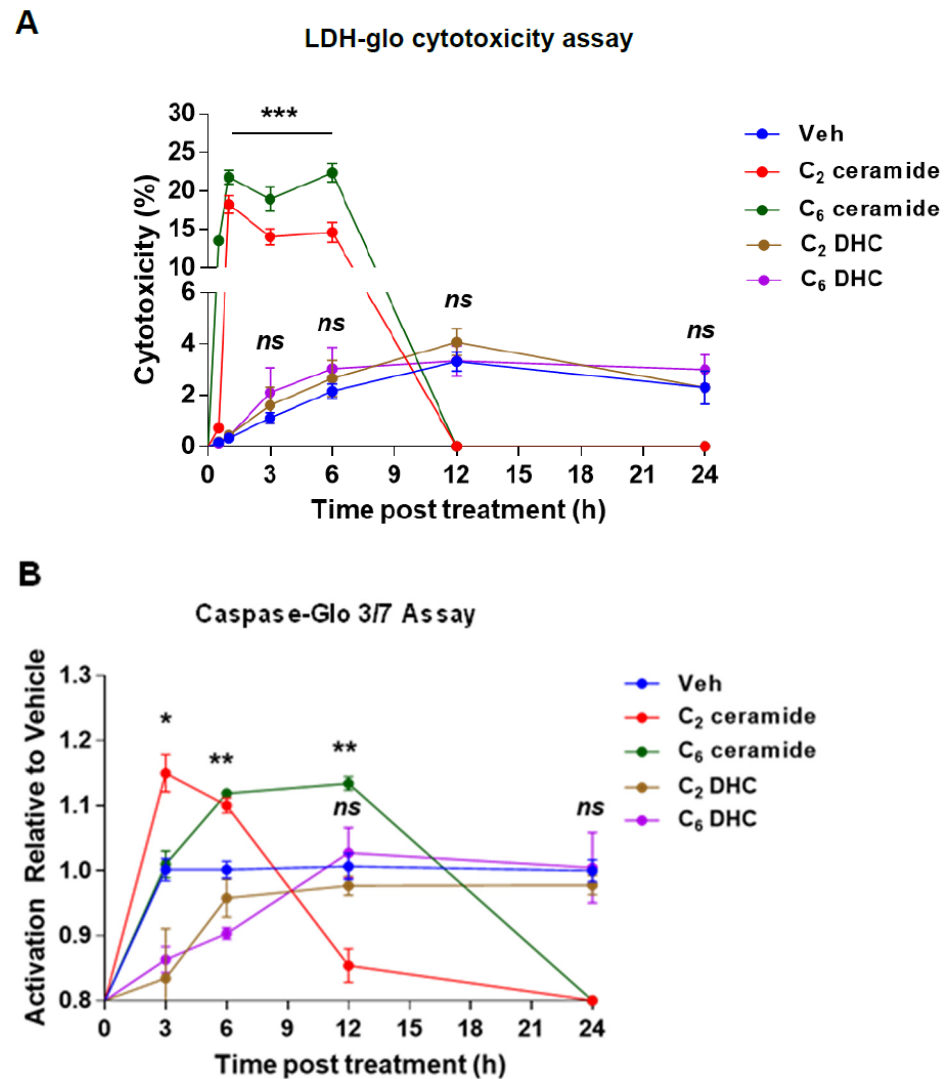


Figure 5. Short-Chain Ceramides induce cytotoxicity and apoptosis in IM-FEN cells. IM-FEN cells were treated with vehicle, 25 μ M C₂-ceramide, C₆-ceramide, C₂-DHC, and C₆-DHC for 30 min, 1-, 3-, 6-, 12-, and 24-h. (A) Cytotoxicity was assessed by the LDH release assay. The percentage of cytotoxicity was calculated relative to the maximum LDH release control (10% Triton[®] X-100). (B) Apoptosis was assessed by measuring Caspase 3/7 activity. The statistical significance of the C₂-ceramide and C₆-ceramide treatment groups is shown with respect to vehicle. Not significant (ns) differences were observed between the vehicle and C₂- and C₆-DHC experimental groups. Results are mean \pm SEM, * $p < 0.05$; ** $p < 0.01$; *** $p < 0.001$.

2.6. TCDD-Induced Cytotoxicity in IM-FEN Cells: The Mediating Role of Ceramides

We found that exposure to TCDD not only precipitates apoptosis in IM-FEN cells but also stimulates the production of ceramides. This linkage was further substantiated by our observations that applying exogenous ceramide directly induces both cytotoxicity and apoptosis in these cells. To delineate the specific role of ceramides in TCDD-induced cytotoxicity in IM-FEN cells, we designed experiments using 10 nM TCDD, applied either

in isolation or combined with 10 μ M myriocin. Myriocin serves as an inhibitor of serine palmitoyltransferase (SPT), the enzyme that catalyzes the rate-limiting step in the de novo ceramide synthesis pathway. These treatments spanned various durations, namely 3, 6, 12, and 24 h, allowing us to assess the cytotoxic effect through the quantification of lactate dehydrogenase (LDH) release into the culture medium.

Our results clearly demonstrated that TCDD exposure incrementally elevates LDH release in IM-FEN cells when compared to vehicle-treated controls. Interestingly, the co-administration of myriocin with TCDD significantly attenuated the TCDD-induced cytotoxic effects, although not completely negating them (Figure 6). This observation suggests the possible involvement of an alternative ceramide synthesis route, such as the N-SMase pathway, in contributing to the cytotoxic effects seen in IM-FEN cells under TCDD influence. These findings highlight the pivotal role of ceramides in mediating the adverse effects of TCDD on the viability of IM-FEN cells, emphasizing the complexity of the underlying mechanisms.

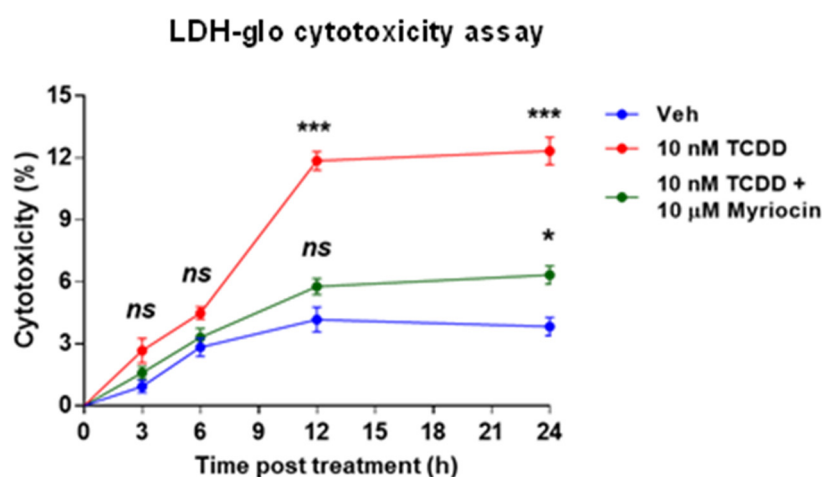


Figure 6. Ceramide involvement in TCDD-induced cytotoxicity in IM-FEN cells. Cells were pretreated with 10 μ M myriocin, an inhibitor of ceramide synthesis, for an hour and then treated with 10 nM TCDD at different time points (3, 6, 12, and 24 h). Cytotoxicity was assessed by the LDH release assay. The percentage of cytotoxicity was calculated relative to the maximum LDH release control (10% Triton[®] X-100). The statistical significance of 10 nM TCDD with or without myriocin is shown with respect to vehicle. Results are mean \pm SEM, * $p < 0.05$; *** $p < 0.001$. ns: Not significant.

2.7. TCDD and Ceramide Impair Neuronal Survival Pathway by Modulating Akt and GSK-3 β Signaling

We have previously shown that exposure to TCDD results in the loss of enteric neurons [9]. This detrimental effect is thought to be mediated by diminished AKT-mediated survival signaling, thereby activating GSK-3 β , two critical components of neuronal cell survival pathways. Additionally, reports have pointed to the influence of ceramide on the PI3K/AKT pathway, with ceramide-induced neuronal apoptosis linked to the dephosphorylation of AKT and GSK-3 β [52,53].

Our study sought to delve into the underlying molecular mechanism responsible for neuronal cell death caused by TCDD and ceramide, with a specific focus on the PI3K/AKT/GSK-3 β pathway. To investigate this further, IM-FEN cells were exposed to varying concentrations of TCDD (0.1, 1, and 10 nM) for 24 h, and the levels of phosphorylated AKT and GSK-3 β were measured using Western blotting.

The results showed a significant decrease in AKT phosphorylation, which is directly correlated with an increase in the active form of GSK-3 β due to its dephosphorylation in the TCDD-treated IM-FEN cells ($p < 0.0001$; Figure 7A,B). This correlation underscores the capability of TCDD to interfere with the AKT-mediated survival signaling pathway, thereby potentiating the role of GSK-3 β in driving neuronal apoptosis.

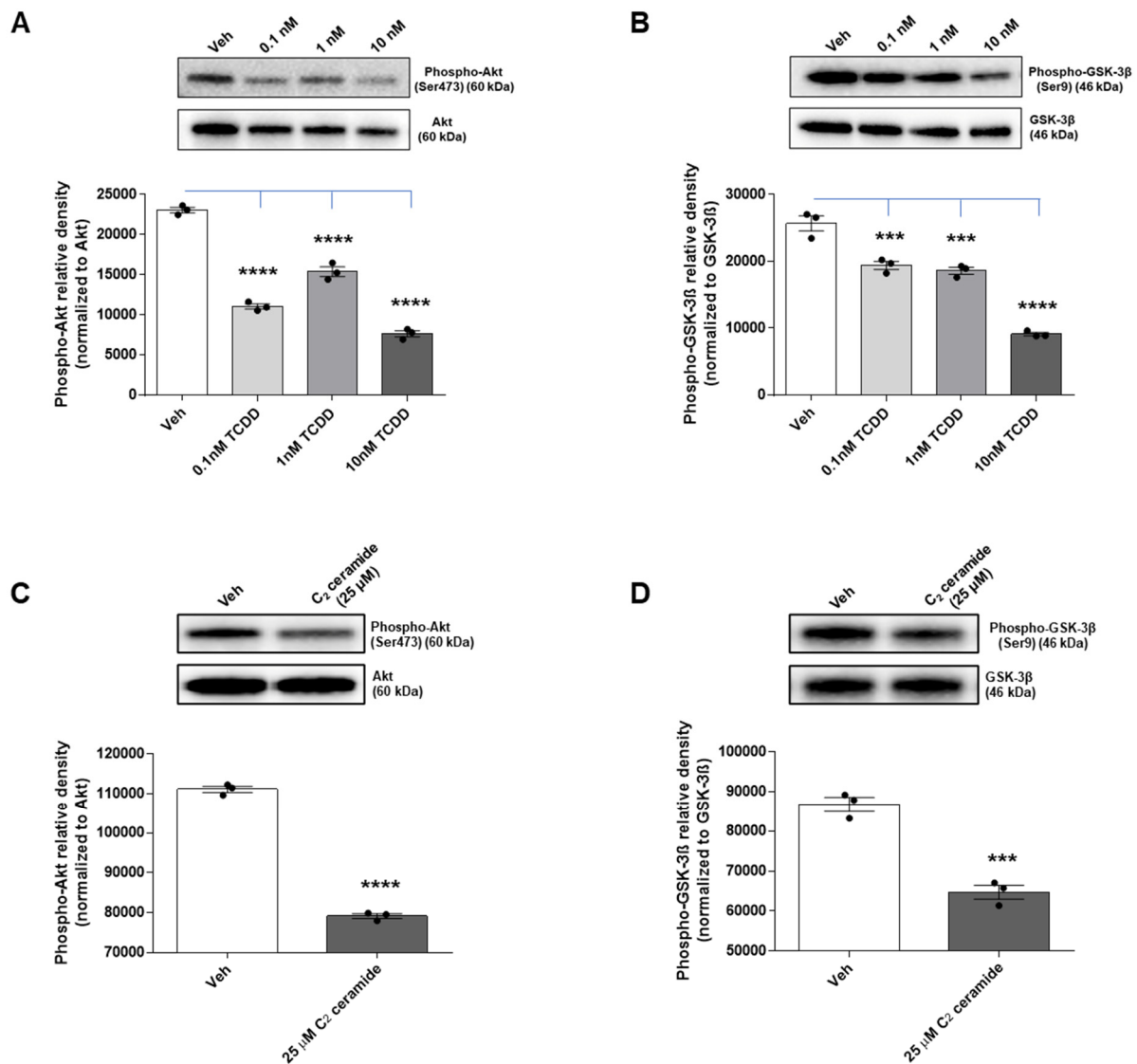


Figure 7. Impact of TCDD and ceramide on neuronal survival pathways via Akt and GSK-3 β modulation. IM-FEN cells were treated with vehicle and various doses of TCDD (0.1, 1, and 10 nM) and C₂ ceramide (25 μ M) for 24 h. Representative images of Phospho-Akt (A,C) and Phospho-GSK-3 β (B,D) Western blots are included. Results from the protein bands' density normalized to corresponding Akt and GSK-3 β have been included in the correspondent graphs. Results are mean \pm SEM, *** $p < 0.001$; **** $p < 0.0001$.

In a parallel study, the impact of ceramide on the AKT survival pathway was examined by treating IM-FEN cells with a vehicle and 25 μ M C₂ ceramide for 24 h. Analysis of AKT and GSK-3 β phosphorylation levels by Western blotting revealed that C₂ ceramide significantly decreased their phosphorylation ($p < 0.0001$; Figure 7C,D). This indicates that ceramide affects the AKT survival pathway by activating GSK-3 β , which is known to induce apoptosis by activating a cascade of reactions involving caspases. These results support the notion that apoptosis in IM-FEN cells induced by TCDD may operate through the suppression of the PI3K/AKT/GSK-3 β survival pathway, with a potential regulatory role played by ceramides.

3. Discussion

We have previously reported that AHR activation by TCDD in the enteric nervous system (ENS) adversely affects nitrergic neurons, leading to delayed intestinal motility due

to TCDD-induced cytotoxicity [9]. In this study, we unveil new insight into the mechanism by which TCDD, a persistent environmental pollutant, induces neurotoxicity via AHR. Our findings demonstrate that TCDD exposure leads to significant apoptosis in IM-FEN cells through a ceramide accumulation pathway, independent of the traditionally implicated endoplasmic reticulum (ER) stress mechanisms. We identified that AHR directly regulates the expression of *Sptlc2* and *Smpd2* in IM-FEN cells, key genes involved in ceramide biosynthesis, highlighting a critical role for AHR in modulating lipid metabolism pathways beyond its established functions. Furthermore, our study elucidates the impact of TCDD on the PI3K/Akt signaling pathway, showing that TCDD exposure results in decreased phosphorylation of AKT and GSK-3 β , key players in cell survival signaling. Taken together, our findings improve understanding of the toxicological mechanisms of TCDD, revealing a novel AHR-mediated pathway that leverages ceramide accumulation to induce apoptosis in enteric neurons, independent of ER stress, and underscores the complexity of the role of AHR in cellular and environmental health.

The AHR controls not only the cellular response to a number of toxic and carcinogenic compounds but also a myriad of physiological functions [54]. Studies have reported that TCDD-induced activation of apoptotic signals occurs in NGF-differentiated pheochromocytoma (dPC12) cells, mouse cerebellar granule cells, primary cultures of cerebral cortical neurons, and zebrafish larvae [7,55–57]. These apoptotic effects are often accompanied by disrupted neuronal function and altered gene expression related to neurodevelopmental processes. In our previous investigation [9], the results demonstrate that TCDD adversely affects nitrergic neurons and thereby contributes to delayed intestinal motility. In our current study, while studying the mechanism underneath this neuronal loss, we noticed that TCDD affects cell survival by inducing apoptosis in enteric neurons. The observed increase in cleaved caspase-3 and cleaved PARP levels in IM-FEN cells treated with TCDD is AHR-mediated and is consistent with the apoptotic effects reported in various cell types exposed to TCDD, thereby providing valuable insights into its toxicological mechanisms [58–61]. Furthermore, the use of the AHR antagonist CH-223191 and cells from neural crest-specific *Ahr*^{-/-} mice (*Wnt1Cre*^{+/-}/*Ahr*^{b(f/f)}) strengthens the evidence for AHR-mediated mechanisms in TCDD-induced cytotoxicity and apoptosis.

Studies have shown that ER stress can lead to apoptosis with subsequent dysregulation of pro-survival and pro-apoptotic gene expression and the possible role of ER stress in neurodegenerative diseases [24,62–64]. Duan et al., studied the role of ER stress in 200 nM TCDD-induced apoptosis in pheochromocytoma (PC12) cells and primary neurons [65]. They found that TCDD-induced ER stress activated the PERK-eIF2 α signaling pathway and triggered apoptosis in PC12 cells. However, our findings suggest that TCDD-induced apoptosis in IM-FEN cells occurs through an ER stress-independent mechanism, as the analysis of ER stress markers did not show significant changes in TCDD-exposed IM-FEN cells. This distinction could stem from differences in cell type, TCDD concentrations, or both, underscoring the complexity of the cytotoxic effects of TCDD.

After excluding ER stress as the triggering mechanism for apoptosis in TCDD-exposed IM-FEN cells, we focused on investigating the potential involvement of ceramides. Ceramides have been recognized as important regulators of apoptosis [66–68]. They can form large protein-permeable channels in the outer membranes of mitochondria, allowing the release of proapoptotic proteins during the initiation of apoptosis [69]. Ceramide accumulation has been observed, leading to caspase activation during apoptosis [70,71] and transcription of apoptosis-related gene products such as Fas ligand and TNF α [72,73]. Recent studies have shown that POPs like TCDD, PCB, and TCDF can regulate sphingolipid metabolism [46,47]. However, the specific role of AHR in ceramide-induced apoptosis is not well understood.

The enzyme serine palmitoyltransferase (SPT) catalyzes the first, rate-limiting step in the de novo ceramide synthesis pathway and is encoded by the genes *Sptlc1* and *Sptlc2*. SPT is likely active as a heterodimer formed with SPT1 and SPT2 [74], with SPT1 primarily playing a role in stabilizing SPT2 rather than contributing to catalytic activity. This

suggests that *Sptlc2* (rather than *Sptlc1*) expression is positively associated with ceramide production. Ceramide is also produced by the hydrolysis of sphingomyelin catalyzed by N-SMase (*Smpd2*, *Smpd3*, and *Smpd4*) in the cell membranes. In our study, chromatin immunoprecipitation (ChIP) assays identified *Sptlc2* and *Smpd2* as potential gene targets of AHR involved in ceramide synthesis. Notably, our results revealed a significant increase in the expression of AHR target genes associated with the de novo ceramide synthesis pathway (*Sptlc1*, *Sptlc2*, *Cers2*, *Cers5*, *Cers6*, and *Degs1*) and the sphingomyelinase pathway (*Smpd2*, *Smpd3*, and *Smpd4*). These changes in gene expression correlated with alterations in the enzymatic activity of N-SMase, resulting in significant changes in ceramide levels and accumulation. This finding expands our understanding of the biological roles of AHR beyond its involvement in detoxification and xenobiotic metabolism, suggesting a broader regulatory role in cellular lipid homeostasis.

Although we did not directly investigate mitochondrial function in terms of ceramide channels or examine the levels of proapoptotic proteins, we evaluated the impact of ceramides on cell survival and apoptosis in IM-FEN cells using exogenous cell-permeable ceramide analogs, C₂- and C₆-ceramides. Short-chain ceramide analogs (C₂- and C₆-ceramides) have been used to mimic ceramide-mediated stress-induced cell death pathways in previous studies [69,75]. Physiological concentrations of ceramides can vary significantly depending on the tissue type, metabolic state, and presence of pathological conditions. The dose selection for C₂- and C₆-ceramides (25 μM) in the study was determined through a comprehensive review of existing literature that investigated the impact of ceramides on neuronal apoptosis [29,76]. These concentrations have been shown to have significant biological effects in previous studies. The differential time points of cytotoxicity and apoptosis effects observed in the study could be attributed to the underlying mechanisms of the assays used to measure these parameters with varying kinetics. LDH is a cytoplasmic enzyme present in viable cells, and its release indicates compromised cell membrane integrity and cellular damage. The time points at which the observed significant LDH release occurs (within the first 1–6 h) suggest that the short-chain ceramides (C₂-ceramide and C₆-ceramide) rapidly induce damage to the cell membrane, leading to the leakage of LDH. Cytotoxicity may primarily result from acute damage to cellular structures. On the other hand, the differences in the timing of caspase 3/7 activation observed with C₂-ceramide and C₆-ceramide treatments (3–6 h and 6–12 h, respectively) suggest that they induce apoptosis through distinct mechanisms or pathways, which may require additional intracellular processes, such as ceramide metabolism or signaling cascades, and that could explain the delayed onset of apoptosis compared to cytotoxicity. The variations in the time points of cytotoxicity and apoptosis could be attributed to subtype-specific effects of these ceramides on the cellular processes involved. Our results indicate that exposure to short-chain ceramides, C₂-ceramide, and C₆-ceramide, induces cytotoxicity and increased caspase 3/7 activity, highlighting the induction of apoptosis in IM-FEN cells. Furthermore, our findings demonstrated that co-treatment of TCDD with myriocin, an inhibitor of ceramide synthesis, restored cell survival, further supporting the role of ceramides in apoptosis. It is important to note that while the chosen concentration of ceramides provides valuable insights into ceramide function, it may not fully replicate the physiological environment. Future studies employing a range of ceramide concentrations would be beneficial to better understand the dose-response relationship and to correlate in vitro findings more accurately with in vivo conditions.

Among the recognized bioactive signaling molecules, sphingolipid metabolites play important roles in signal transduction and cell regulation [77,78]. Ceramides can modulate cell death by inhibiting the PI3K antiapoptotic/prosurvival pathway, which involves the regulation of AKT activity [44]. However, the specific role of AHR in ceramide-induced apoptosis is not well understood. Phosphatidylinositol 3-kinase (PI3K) and its downstream effector, the protein-serine/threonine kinase AKT, a negative regulator of GSK-3β, play an important role in preventing apoptosis by blocking the activation of the caspase cascade in several cell types, including neuronal and glial cells [29,79–83]. Reports have suggested

that ceramides affect the PI3K/AKT pathway [52,53,72,84]. In our research, we aimed to investigate the underlying molecular mechanism responsible for neuronal cell death induced by TCDD and ceramide, with a specific focus on the PI3K/AKT/GSK-3 β pathway. Our findings reveal a significant reduction in the phosphorylation levels of both AKT and GSK-3 β in TCDD-treated and C₂ ceramide-treated IM-FEN cells. This implies that TCDD and ceramides adversely impact the activation and functioning of AKT and GSK-3 β in enteric neuronal cells, thereby shedding light on the potential mechanisms contributing to the observed neuronal loss associated with TCDD exposure.

In summary, this study addresses a critical gap in our understanding of TCDD-induced enteric neurotoxicity by elucidating the underlying molecular mechanisms and identifying potential targets for therapeutic intervention. Our findings lay the groundwork for future studies exploring the regulatory role of AHR in apoptosis and sphingolipid metabolism. This could lead to a broader understanding of the environmental factors influencing neurodegenerative diseases and other conditions associated with dysregulated apoptosis. The primary limitation of our study is its focus on *in vitro* models (IM-FEN cells). While these models provide valuable insights into cellular mechanisms, the findings need validation in *in vivo* models to establish their physiological relevance and the potential for therapeutic applications. Our study demonstrates a novel pathway for TCDD-induced apoptosis via ceramide accumulation (Figure 8). Future studies will examine additional alternative pathways that could also contribute to TCDD-induced apoptosis. Further research could provide a more comprehensive understanding of the cellular response to TCDD exposure. While the study identifies *Sptlc2* and *Smpd2* as AHR targets in the regulation of ceramide synthesis, the potential existence of other critical targets or mechanisms involved in this process is not fully explored. Future studies could uncover additional layers of regulation. The study suggests potential therapeutic targets for mitigating TCDD-induced toxicity, but it does not provide direct evidence of efficacy in preventing or reversing the effects of TCDD exposure. Further research is needed to develop and test specific interventions based on these targets. Despite these limitations, our study makes a significant contribution to our understanding of the mechanisms by which environmental pollutants induce neurotoxicity and opens new avenues for research and therapeutic development.

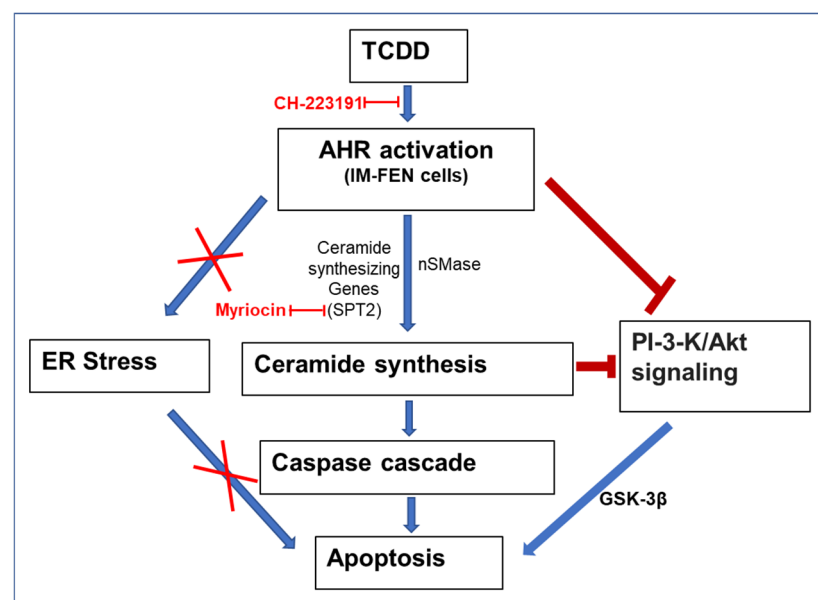


Figure 8. A proposed model showing enhanced ceramide synthesis leading to apoptosis in IM-FEN cells. Key components showing activators in blue arrows and inhibitory associations in red lines.

4. Materials and Methods

4.1. Mice

Ahr floxed mice (*Ahr*^(fl/fl)) were generated by Cyagen Biosciences, Inc., by flanking exons 5 to 7 with *loxP* sites. *Ahr*^(fl/fl) mice were subsequently backcrossed 10 generations to C57Bl/6J mice and confirmed by the Genome Scanning Services of the Jackson Laboratory to have >99% C57Bl/6J background (*Ahr*^{b(fl/fl)}). *Wnt1-Cre* transgenic mice that express Cre recombinase (*B6.Cg-E2f1*^{Tg(Wnt1-cre)2Sor/J}) were purchased from Jackson Laboratory. *Ahr* was specifically deleted in neural crest cells by crossing *Ahr*^{b(fl/fl)} mice with *Wnt1-cre* mice. The offspring were genotyped using primers (Integrated DNA Technologies, Coralville, IA, USA) listed in Table 3 to confirm that they were homozygous for the *Ahr*^b floxed gene and either hemizygous (*Wnt1Cre*^{+/-}/*Ahr*^{b(fl/fl)}) or negative for *Wnt1-cre* (*Wnt1Cre*^{-/-}/*Ahr*^{b(fl/fl)}) mice. *Wnt1Cre*^{-/-}/*Ahr*^{b(fl/fl)} mice were used as controls. All experimental mice used were 8- to 10-week-old male mice. Animal studies were approved by the Institutional Animal Care and Use Committee at Pennsylvania State University and performed according to the university guidelines for the ethical treatment of animals.

Table 3. Primers used for genotyping.

Gene	Forward Primer (5'→3')	Reverse Primer (5'→3')
<i>Ahr</i>	AAGGCCACTAAAGCAATGGGATGT	AAAGTTTATGACTGGGTCACCACA
<i>Wnt1Cre</i>	CAGCGCCGCAACTATAAGAG	CATCGACCGGTAATGCAG

4.2. Cell Culture

In vitro experiments were conducted using Immortal fetal enteric neuronal cells [48]. These cells were cultured in a modified N2 medium [85] prepared with DMEM/F-12 (Thermo Fisher Scientific, Waltham, MA, USA) containing 10 ng/mL glial cell line-derived neurotrophic factor (GDNF) (Shenandoah Biotechnology, Inc., Warminster, PA, USA), 10% fetal bovine serum (FBS) (Bio-Techne, Minneapolis, MN, USA), and 20 U/mL recombinant mouse interferon- γ (MilliporeSigma, Burlington, MA, USA). The culture was maintained in a humidified tissue culture incubator with 10% CO₂ at a permissive temperature of 33 °C for 24 to 48 h, allowing the cells to proliferate until confluent monolayers were formed. Subsequently, the medium was replaced with neurobasal-A medium (NBM) supplemented with B-27 serum-free supplement (Thermo Fisher Scientific, Waltham, MA, USA), 1 mmol/L glutamine (Thermo Fisher Scientific, Waltham, MA, USA), 1% FBS, and 10 ng/mL GDNF. The cells were then transferred to an atmosphere of 5% CO₂ at 39 °C to allow differentiation for 48 h. After differentiation, the cells were cultured on poly-D-lysine and laminin-coated plates (Corning, NY, USA) and treated with various doses of TCDD (0.1, 1, and 10 nM) (Cambridge Isotope Laboratories, Inc., Tewksbury, MA, USA) at different time intervals (3, 6, 12, and 24 h).

4.3. Primary Culture Preparation

Primary cultures of mouse ileum and colonic myenteric neurons were prepared following previously published protocols [86,87], using 8-week-old *Wnt1Cre*^{+/-}/*Ahr*^{b(fl/fl)} and *Wnt1Cre*^{-/-}/*Ahr*^{b(fl/fl)} mice. Myenteric neurons were seeded onto poly-L-lysine-coated 12 mm coverslips and cultured at 37 °C with 5% CO₂ in complete NBM, as described earlier. The medium was partially replaced every 24 h. After 5 days in culture, the neurons were treated with 10 nM TCDD for 24 h.

4.4. LDH-Glo Cytotoxicity Assay

Immortal fetal enteric neuronal cells were cultured on 96-well white plates with clear bottoms (10,000 cells/well) at 39 °C and treated with vehicle, 10 nM TCDD with or without 10 μ M CH-223191 (MilliporeSigma, Burlington, MA, USA), a potent and specific antagonist of AHR, and 10 μ M Myriocin (MilliporeSigma, Burlington, MA, USA), a potent inhibitor of SPT, the rate-limiting enzyme of ceramide biosynthesis, and 25 μ M C₂- and C₆-ceramides

and dihydroceramides (Enzo Life Sciences, Inc., Farmingdale, NY, USA) in complete NBM for different time points (0.5, 1, 3, 6, 12, 24 h). Cells were pretreated with 10 μ M CH-223191 and 10 μ M Myriocin for 1 h prior to the addition of 10 nM TCDD. The percentage of cytotoxicity was calculated relative to the maximum lactate dehydrogenase (LDH) release control (10% Triton[®] X-100) as recommended by the manufacturer's instructions using the LDH-Glo Cytotoxicity Assay kit from Promega (Madison, WI, USA).

4.5. Caspase-Glo 3/7 Assay

Immorto fetal enteric neuronal cells were cultured on 96-well white plates with clear bottoms (10,000 cells/well) at 39 °C and treated with vehicle, 10 nM TCDD with or without 10 μ M CH-223191, 25 μ M C₂- and C₆-ceramides and dihydroceramides (Enzo Life Sciences, Inc., Farmingdale, NY, USA) in complete NBM for different time points (0.5, 1, 3, 6, 12, 24 h). Cells were pretreated with 10 μ M CH-223191 for 1 h prior to the addition of 10 nM TCDD. Caspase 3/7 activity was assessed using the Caspase-Glo 3/7 Assay kit from Promega (Madison, WI, USA), in accordance with the manufacturer's protocol. Luminometer readings were taken 1 h after the addition of the Caspase-Glo 3/7 Reagent.

4.6. Real-Time PCR

Immorto fetal enteric neuronal cells cultured on poly-D-lysine and laminin-coated 6-well plates (160,000 cells/well) at 39 °C were treated with vehicle and 10 nM TCDD at various time points (0.5, 1, 3, 6, 12, 24 h). Total RNA was extracted using TRIzol Reagent (Thermo Fisher Scientific, Waltham, MA, USA) according to the manufacturer's instructions. Complementary DNA (cDNA) was synthesized from 1 μ g of total RNA using the qScript cDNA SuperMix (Quantabio, Beverly, MA, USA). Quantitative real-time PCR was performed with cDNA using PowerUp SYBR Green Master Mix (Applied Biosystems, Waltham, MA, USA) on the QuantStudio 3 Real-Time PCR System (Applied Biosystems, Waltham, MA, USA) with primers listed in Table 1. The Ct values obtained were normalized to the housekeeping gene B2M.

4.7. ChIP-PCR/qPCR Assay

The ChIP-PCR/qPCR assay was conducted by the SimpleChIP[®] Plus Enzymatic Chromatin IP Kit (Magnetic Beads) according to the manufacturer's instructions (Cell Signaling Technology, Danvers, MA, USA). Briefly, IM-FEN cells cultured on 15 cm dishes (4×10^6 cells/dish) at 39 °C were treated with vehicle and 10 nM TCDD for 1 h were collected, and, proteins and DNA were cross-linked with 1% formaldehyde in PBS at room temperature for 10 min. Chromatin was extracted and immunoprecipitated with 2 μ g of antibodies to AHR (Enzo, BML-SA210-0100) at 4 °C overnight. The immune complexes were collected by incubation with protein G magnetic beads, and the beads were washed with low salt, high salt, and ChIP buffer. After the elution of bound chromatin, the genomic DNA was purified using a spin column and subjected to PCR or qPCR using primers specific for the *Cyp1a1*, *Sptlc2*, and *Smpd2* promoter regions, which are known to contain DREs, or the non-binding region as a negative control (Table 2).

4.8. Sphingomyelinase Assay

Immorto fetal enteric neuronal cells were cultured in 96-well plates (10,000 cells/well) at 39 °C and treated with vehicle and 10 nM TCDD for 24 h. Neutral sphingomyelinase (N-SMase) activity was measured using a colorimetric sphingomyelinase assay kit from Sigma (Burlington, MA, USA) according to the manufacturer's protocol.

4.9. Orbitrap-MS Analysis of Lipids

IM-FEN cells cultured on 10 cm dishes (2×10^6 cells/dish) at 39 °C were treated with vehicle, and 10 nM TCDD for 3 h were collected and extracted twice with 1.0 mL of pre-cooled isopropanol/water/ethyl acetate (30:10:60, v:v:v) containing 1:1000 Equisplash (Avanti Polar Lipids, Alabaster, AL, USA). After sonication and centrifugation (Eppendorf,

Hamburg, Germany), the supernatant was collected, evaporated to dryness (SpeedVac, Thermo Scientific, Waltham, MA, USA), and dissolved in 60 μ L of isopropanol/acetonitrile/ H_2O (45:35:20, *v:v:v*). After centrifugation, the supernatants were transferred to autosampler vials for LC-MS analysis.

Total lipids were analyzed by a Vanquish UHPLC system coupled to an Orbitrap Fusion Lumos TribridTM mass spectrometer using a H-ESITM ion source (all Thermo Fisher Scientific) with a Waters (Milford, MA, USA) CSH C18 column (1.0 \times 150 mm; 1.7 μ m particle size) as previously described [88]. LC-MS data were analyzed by the open-source software MS-DIAL ver. 4.9.221218 [89], identifications were performed using the in-silico lipid library, and the spectra were manually checked to confirm assignments. The experiment was processed in technical duplicate, and the averages were used for statistical purposes.

4.10. Western Blotting

Cell lysates were obtained from IM-FEN cells cultured on poly-D-lysine and laminin-coated 6-well plates (160,000 cells/well) at 39 °C and treated with or without TCDD (0.1, 1, and 10 nM) and C_2 ceramide (25 μ M) for 24 h. Additionally, some cells were pre-treated with the AHR antagonist CH-223191 (10 μ M) for one hour before a 24-h exposure to 10 nM TCDD. Thapsigargin (300 nM, 5-h treatment) (MilliporeSigma, Burlington, MA, USA) was used as a positive control to benchmark ER stress. Proteins (15 μ g per lane) were loaded onto a 4–20% sodium dodecyl sulfate–polyacrylamide gel electrophoresis (Bio-Rad, Hercules, CA, USA) and transferred to a PVDF membrane. The membranes were probed for Cleaved caspase-3, Cleaved PARP, Phospho-Akt (Ser473), Akt, Phospho-GSK-3 β (Ser9), GSK-3 β , and ER stress-associated proteins, including GRP78, IRE1 α , and CHOP, using respective specific antibodies (Table 4). GAPDH was used as a loading control. Band intensity was measured semiquantitatively using the Scion Image software (<https://scion-image.software.informer.com/> accessed on 25 July 2024) (Scion Corporation, Frederick, MD, USA) and expressed as a ratio of band intensity relative to the loading control.

Table 4. Antibodies used in Western blot (WB) and immunofluorescence (IF).

Antibody/Host	Company	Cat. No.	Dilution
Cleaved Caspase-3 (Asp175)	Cell Signaling Technology (Danvers, MA, USA)	9661	1:1000 (WB) 1:200 (IF)
Cleaved PARP (Asp214)	Cell Signaling Technology	94885	1:1000 (WB)
Phospho-Akt (Ser473)	Cell Signaling Technology	9271	1:1000 (WB)
Akt	Cell Signaling Technology	9272	1:1000 (WB)
Phospho-GSK-3 β (Ser9)	Cell Signaling Technology	9336	1:1000 (WB)
GSK-3 β	Cell Signaling Technology	12456	1:1000 (WB)
BiP (C50B12)	Cell Signaling Technology	3177	1:1000 (WB)
IRE1 α (14C10)	Cell Signaling Technology	3294	1:1000 (WB)
CHOP (D46F1)	Cell Signaling Technology	5554	1:1000 (WB)
GAPDH/Rabbit	Cell Signaling Technology	2118	1:2500 (WB)
TUJ1/Mouse	abcam (Waltham, MA, USA)	ab78078	1:500 (IF)
HRP-conjugated anti-mouse	Cell Signaling Technology	7076	1:2000 (WB)
HRP-conjugated anti-rabbit	Cell Signaling Technology	7074	1:2000–5000 (WB)
Goat anti-Rb, Alexa Fluor 488	Invitrogen (Waltham, MA, USA)	A11008	1:200 (IF)
Goat anti-Mouse, Alexa Fluor 594	Invitrogen (Waltham, MA, USA)	A11005	1:200 (IF)

4.11. TUNEL Staining

Immorto fetal enteric neuronal cells cultured on poly-L-lysine coated 12 mm coverslips (20,000 cells/well) (Neuvitro Corporation, Camas, WA, USA) were treated with vehicle and 10 nM TCDD for 24 h. To detect apoptosis, terminal deoxynucleotidyl transferase dUTP

nick end labeling (TUNEL) staining was performed using the In Situ Cell Death Detection Kit, Fluorescein (Roche Diagnostics, Indianapolis, IN, USA), following the manufacturer's protocol. The cells were counterstained with enteric neuronal marker TUJ1 in conjunction with Alexa Fluor 594 (Table 4) and nuclear dye DAPI (AnaSpec, Fremont, CA, USA). Images were captured on a Revolve R4 Microscope (ECHO, San Diego, CA, USA).

4.12. Immunofluorescence Staining of Primary Culture Cells

Myenteric neurons from *Wnt1Cre^{+/-}/Ahr^{b(f/f)}* and *Wnt1Cre^{-/-}/Ahr^{b(f/f)}* mice were cultured on poly-L-lysine coated 12 mm coverslips (20,000 cells/well) and treated with vehicle or 10 nM TCDD for 24 h at 37 °C. Following treatment, the cells were fixed using 4% paraformaldehyde for 20 min and then blocked for 1 h with a blocking and permeabilization solution containing 0.3% Triton X-100 and 5% BSA (MilliporeSigma, Burlington, MA, USA) in PBS. The cells were then incubated with primary antibodies (TUJ1 and cleaved caspase-3, as listed in Table 4) at room temperature for 2 h. Secondary detection was performed in conjunction with Alexa Fluor 594 or 488. Images were captured with a Revolve R4 Microscope (ECHO, CA).

4.13. Statistical Analysis

Data analysis was performed using GraphPad Prism version 9.1.1 (GraphPad, San Diego, CA, USA). Statistical analysis for two treatment groups was conducted using the Student's *t*-test. For multiple data sets, one-way analysis of variance (ANOVA) was employed, followed by Tukey's multiple comparison test. Results are presented as mean ± SEM, with a *p*-value of 0.05 or less considered statistically significant.

Author Contributions: Conceptualization, M.A., G.H.P., S.S. and A.D.P.; Methodology, S.M.K.; Formal analysis, I.K.; Investigation, M.A., S.M.K. and A.D.P.; Resources, A.D.P.; Writing—original draft, M.A. and A.D.P.; Writing—review & editing, I.K., G.H.P. and S.S.; Supervision, A.D.P.; Funding acquisition, A.D.P. All authors have read and agreed to the published version of the manuscript.

Funding: A.D.P. was supported by the National Institute of Environmental Health Sciences (NIEHS) grants (ES035027, S10OD021750), the PA Department of Health using Tobacco funds, and the USDA National Institute of Food and Federal Appropriations under Project PEN047702 and Accession number 7006412. G.H.P. was supported by NIEHS R35 ES028244.

Data Availability Statement: Data is contained within the article.

Conflicts of Interest: The authors declare no conflict of interest.

References

1. Van Den Berg, M.; Birnbaum, L.S.; Denison, M.; De Vito, M.; Farland, W.; Feeley, M.; Fiedler, H.; Håkansson, H.; Hanberg, A.; Haws, L.; et al. The 2005 World Health Organization Reevaluation of Human and Mammalian Toxic Equivalency Factors for Dioxins and Dioxin-Like Compounds. *Toxicol. Sci.* **2006**, *93*, 223–241. [[CrossRef](#)] [[PubMed](#)]
2. Berg, M.V.D.; De Jongh, J.; Poiger, H.; Olson, J.R. The Toxicokinetics and Metabolism of Polychlorinated Dibenzo-p-Dioxins (PCDDs) and Dibenzofurans (PCDFs) and Their Relevance for Toxicity. *Crit. Rev. Toxicol.* **1994**, *24*, 1–74. [[CrossRef](#)] [[PubMed](#)]
3. Knerr, S.; Schrenk, D. Carcinogenicity of 2,3,7,8-tetrachlorodibenzo-p-dioxin in experimental models. *Mol. Nutr. Food Res.* **2006**, *50*, 897–907. [[CrossRef](#)] [[PubMed](#)]
4. Hogaboam, J.P.; Moore, A.J.; Lawrence, B.P. The Aryl Hydrocarbon Receptor Affects Distinct Tissue Compartments during Ontogeny of the Immune System. *Toxicol. Sci.* **2007**, *102*, 160–170. [[CrossRef](#)] [[PubMed](#)]
5. Marshall, N.B.; Kerkvliet, N.I. Dioxin and immune regulation. *Ann. N. Y. Acad. Sci.* **2010**, *1183*, 25–37. [[CrossRef](#)] [[PubMed](#)]
6. Zhang, T.; Zhou, X.; Ren, X.; Zhang, X.; Wu, J.; Wang, S.; Wang, Z. Animal Toxicology Studies on the Male Reproductive Effects of 2,3,7,8-Tetrachlorodibenzo-p-Dioxin: Data Analysis and Health Effects Evaluation. *Front. Endocrinol.* **2021**, *12*, 696106. [[CrossRef](#)] [[PubMed](#)]
7. Tomasini, M.C.; Beggiano, S.; Ferraro, L.; Tanganelli, S.; Marani, L.; Lorenzini, L.; Antonelli, T. Prenatal exposure to 2,3,7,8-tetrachlorodibenzo-p-dioxin produces alterations in cortical neuron development and a long-term dysfunction of glutamate transmission in rat cerebral cortex. *Neurochem. Int.* **2012**, *61*, 759–766. [[CrossRef](#)] [[PubMed](#)]
8. Urban, P.; Pelclová, D.; Lukáš, E.; Kupka, K.; Preiss, J.; Fenclová, Z.; Šmerhovský, Z. Neurological and neurophysiological examinations on workers with chronic poisoning by 2,3,7,8-TCDD: Follow-up 35 years after exposure. *Eur. J. Neurol.* **2007**, *14*, 213–218. [[CrossRef](#)] [[PubMed](#)]

9. Vijay, A.; Boyle, N.R.; Kumar, S.M.; Perdew, G.H.; Srinivasan, S.; Patterson, A.D. Aryl hydrocarbon receptor activation affects nitrenergic neuronal survival and delays intestinal motility in mice. *Toxicol. Sci.* **2023**, *192*, 117–128. [[CrossRef](#)]
10. Zhou, X.; Chakraborty, D.; Murray, I.A.; Coslo, D.; Kehs, Z.; Vijay, A.; Ton, C.; Desai, D.; Amin, S.G.; Patterson, A.D.; et al. Aryl Hydrocarbon Receptor Activation Coordinates Mouse Small Intestinal Epithelial Cell Programming. *Mod. Pathol.* **2023**, *103*, 100012. [[CrossRef](#)]
11. Nebert, D.W. Aryl hydrocarbon receptor (AHR): “pioneer member” of the basic-helix/loop/helix per-Arnt-sim (bHLH/PAS) family of “sensors” of foreign and endogenous signals. *Prog. Lipid Res.* **2017**, *67*, 38–57. [[CrossRef](#)] [[PubMed](#)]
12. Raggi, F.; Russo, D.; Urbani, C.; Sardella, C.; Manetti, L.; Cappellani, D.; Lupi, I.; Tomisti, L.; Martino, E.; Marcocci, C.; et al. Divergent Effects of Dioxin- or Non-Dioxin-Like Polychlorinated Biphenyls on the Apoptosis of Primary Cell Culture from the Mouse Pituitary Gland. *PLoS ONE* **2016**, *11*, e0146729. [[CrossRef](#)] [[PubMed](#)]
13. Tomblin, J.K.; Salisbury, T.B. Insulin like growth factor 2 regulation of aryl hydrocarbon receptor in MCF-7 breast cancer cells. *Biochem. Biophys. Res. Commun.* **2013**, *443*, 1092–1096. [[CrossRef](#)] [[PubMed](#)]
14. Yang, E.-J.; Stokes, J.V.; Kummari, E.; Eells, J.; Kaplan, B.L. Immunomodulation by Subchronic Low Dose 2,3,7,8-Tetrachlorodibenzo-p-Dioxin in Experimental Autoimmune Encephalomyelitis in the Absence of Pertussis Toxin. *Toxicol. Sci.* **2016**, *151*, 35–43. [[CrossRef](#)] [[PubMed](#)]
15. Gutiérrez-Vázquez, C.; Quintana, F.J. Regulation of the Immune Response by the Aryl Hydrocarbon Receptor. *Immunity* **2018**, *48*, 19–33. [[CrossRef](#)] [[PubMed](#)]
16. Vogel, C.F.A.; Van Winkle, L.S.; Esser, C.; Haarmann-Stemmann, T. The aryl hydrocarbon receptor as a target of environmental stressors—Implications for pollution mediated stress and inflammatory responses. *Redox Biol.* **2020**, *34*, 101530. [[CrossRef](#)] [[PubMed](#)]
17. Kolluri, S.K.; Jin, U.-H.; Safe, S. Role of the aryl hydrocarbon receptor in carcinogenesis and potential as an anti-cancer drug target. *Arch. Toxicol.* **2017**, *91*, 2497–2513. [[CrossRef](#)] [[PubMed](#)]
18. Huang, Y.; He, J.; Liang, H.; Hu, K.; Jiang, S.; Yang, L.; Mei, S.; Zhu, X.; Yu, J.; Kijlstra, A.; et al. Aryl Hydrocarbon Receptor Regulates Apoptosis and Inflammation in a Murine Model of Experimental Autoimmune Uveitis. *Front. Immunol.* **2018**, *9*, 1713. [[CrossRef](#)] [[PubMed](#)]
19. Kajta, M.; Wójtowicz, A.; Maćkowiak, M.; Lason, W. Aryl hydrocarbon receptor-mediated apoptosis of neuronal cells: A possible interaction with estrogen receptor signaling. *Neuroscience* **2009**, *158*, 811–822. [[CrossRef](#)]
20. Bredesen, D.E. Apoptosis: Overview and Signal Transduction Pathways. *J. Neurotrauma* **2000**, *17*, 801–810. [[CrossRef](#)]
21. Eldadah, B.A.; Faden, A.I. Caspase Pathways, Neuronal Apoptosis, and CNS Injury. *J. Neurotrauma* **2000**, *17*, 811–829. [[CrossRef](#)] [[PubMed](#)]
22. Rong, F.; Gao, X.; Liu, K.; Wu, J. Methotrexate remediates spinal cord injury in vivo and in vitro via suppression of endoplasmic reticulum stress-induced apoptosis. *Exp. Ther. Med.* **2018**, *15*, 4191–4198. [[CrossRef](#)] [[PubMed](#)]
23. Han, Y.; Yuan, M.; Guo, Y.-S.; Shen, X.-Y.; Gao, Z.-K.; Bi, X. Mechanism of Endoplasmic Reticulum Stress in Cerebral Ischemia. *Front. Cell Neurosci.* **2021**, *15*, 704334. [[CrossRef](#)] [[PubMed](#)]
24. Lindholm, D.; Wootz, H.; Korhonen, L. ER stress and neurodegenerative diseases. *Cell Death Differ.* **2006**, *13*, 385–392. [[CrossRef](#)] [[PubMed](#)]
25. Galehdar, Z.; Swan, P.; Fuerth, B.; Callaghan, S.M.; Park, D.S.; Cregan, S.P. Neuronal Apoptosis Induced by Endoplasmic Reticulum Stress Is Regulated by ATF4–CHOP-Mediated Induction of the Bcl-2 Homology 3-Only Member PUMA. *J. Neurosci.* **2010**, *30*, 16938–16948. [[CrossRef](#)] [[PubMed](#)]
26. Yu, A.-R.; Jeong, Y.J.; Hwang, C.Y.; Yoon, K.-S.; Choe, W.; Ha, J.; Kim, S.S.; Pak, Y.K.; Yeo, E.-J.; Kang, I. Alpha-naphthoflavone induces apoptosis through endoplasmic reticulum stress via c-Src-, ROS-, MAPKs-, and arylhydrocarbon receptor-dependent pathways in HT22 hippocampal neuronal cells. *NeuroToxicology* **2018**, *71*, 39–51. [[CrossRef](#)]
27. Koybasi, S.; Senkal, C.E.; Sundararaj, K.; Spassieva, S.; Bielawski, J.; Osta, W.; Day, T.A.; Jiang, J.C.; Jazwinski, S.M.; Hannun, Y.A.; et al. Defects in Cell Growth Regulation by C18:0-Ceramide and Longevity Assurance Gene 1 in Human Head and Neck Squamous Cell Carcinomas. *J. Biol. Chem.* **2004**, *279*, 44311–44319. [[CrossRef](#)] [[PubMed](#)]
28. Kagan, T.; Stoyanova, G.; Lockshin, R.A.; Zakeri, Z. Ceramide from sphingomyelin hydrolysis induces neuronal differentiation, whereas de novo ceramide synthesis and sphingomyelin hydrolysis initiate apoptosis after NGF withdrawal in PC12 Cells. *Cell Commun. Signal* **2022**, *20*, 15. [[CrossRef](#)]
29. Czubowicz, K.; Strosznajder, R. Ceramide in the Molecular Mechanisms of Neuronal Cell Death. The Role of Sphingosine-1-Phosphate. *Mol. Neurobiol.* **2014**, *50*, 26–37. [[CrossRef](#)]
30. Plotegher, N.; Bubacco, L.; Greggio, E.; Civiero, L. Ceramides in Parkinson’s Disease: From Recent Evidence to New Hypotheses. *Front. Neurosci.* **2019**, *13*, 330. [[CrossRef](#)]
31. Mandon, E.; Ehses, I.; Rother, J.; van Echten, G.; Sandhoff, K. Subcellular localization and membrane topology of serine palmitoyltransferase, 3-dehydrosphinganine reductase, and sphinganine N-acyltransferase in mouse liver. *J. Biol. Chem.* **1992**, *267*, 11144–11148. [[CrossRef](#)] [[PubMed](#)]
32. Bose, R.; Verheij, M.; Haimovitz-Friedman, A.; Scotto, K.; Fuks, Z.; Kolesnick, R. Ceramide synthase mediates daunorubicin-induced apoptosis: An alternative mechanism for generating death signals. *Cell* **1995**, *82*, 405–414. [[CrossRef](#)] [[PubMed](#)]

33. Bionda, C.; Portoukalian, J.; Schmitt, D.; Rodriguez-Lafresse, C.; Ardail, D. Subcellular compartmentalization of ceramide metabolism: MAM (mitochondria-associated membrane) and/or mitochondria? *Biochem. J.* **2004**, *382*, 527–533. [[CrossRef](#)] [[PubMed](#)]
34. Shimeno, H.; Soeda, S.; Sakamoto, M.; Kouchi, T.; Kowakame, T.; Kihara, T. Partial purification and characterization of sphingosine N-acyltransferase (ceramide synthase) from bovine liver mitochondrion-rich fraction. *Lipids* **1998**, *33*, 601–605. [[CrossRef](#)] [[PubMed](#)]
35. Jarvis, W.D.; Kolesnick, R.N.; A Fornari, F.; Traylor, R.S.; A Gewirtz, D.; Grant, S. Induction of apoptotic DNA damage and cell death by activation of the sphingomyelin pathway. *Proc. Natl. Acad. Sci. USA* **1994**, *91*, 73–77. [[CrossRef](#)] [[PubMed](#)]
36. Gillard, B.K.; Clement, R.G.; Marcus, D.M. Variations among cell lines in the synthesis of sphingolipids in de novo and recycling pathways. *Glycobiology* **1998**, *8*, 885–890. [[CrossRef](#)] [[PubMed](#)]
37. Dbaibo, G.S.; El-Assaad, W.; Krikorian, A.; Liu, B.; Diab, K.; Idriss, N.Z.; El-Sabban, M.; A Driscoll, T.; Perry, D.K.; A Hannun, Y. Ceramide generation by two distinct pathways in tumor necrosis factor α -induced cell death. *FEBS Lett.* **2001**, *503*, 7–12. [[CrossRef](#)] [[PubMed](#)]
38. Haimovitz-Friedman, A.; Kan, C.C.; Ehleiter, D.; Persaud, R.S.; McLoughlin, M.; Fuks, Z.; Kolesnick, R.N. Ionizing radiation acts on cellular membranes to generate ceramide and initiate apoptosis. *J. Exp. Med.* **1994**, *180*, 525–535. [[CrossRef](#)] [[PubMed](#)]
39. Dbaibo, G.S.; Pushkareva, M.Y.; A Rachid, R.; Alter, N.; Smyth, M.J.; Obeid, L.M.; A Hannun, Y. p53-dependent ceramide response to genotoxic stress. *J. Clin. Investig.* **1998**, *102*, 329–339. [[CrossRef](#)]
40. Rotolo, J.A.; Zhang, J.; Donepudi, M.; Lee, H.; Fuks, Z.; Kolesnick, R. Caspase-dependent and -independent Activation of Acid Sphingomyelinase Signaling. *J. Biol. Chem.* **2005**, *280*, 26425–26434. [[CrossRef](#)]
41. Fillet, M.; Bentires-Alj, M.; Derogowski, V.; Greimers, R.; Gielen, J.; Piette, J.; Bours, V.; Merville, M.-P. Mechanisms involved in exogenous C2- and C6-ceramide-induced cancer cell toxicity. *Biochem. Pharmacol.* **2003**, *65*, 1633–1642. [[CrossRef](#)]
42. Ghidoni, R.; Sala, G.; Giuliani, A. Use of sphingolipid analogs: Benefits and risks. *Biochim. Biophys. Acta.* **1999**, *1439*, 17–39. [[CrossRef](#)] [[PubMed](#)]
43. Obeid, L.M.; Linardic, C.M.; Karolak, L.A.; Hannun, Y.A. Programmed Cell Death Induced by Ceramide. *Science* **1993**, *259*, 1769–1771. [[CrossRef](#)] [[PubMed](#)]
44. A Stoica, B.; A Movsesyan, V.; Iv, P.M.L.; I Faden, A. Ceramide-induced neuronal apoptosis is associated with dephosphorylation of Akt, BAD, FKHR, GSK-3 β , and induction of the mitochondrial-dependent intrinsic caspase pathway. *Mol. Cell Neurosci.* **2003**, *22*, 365–382. [[CrossRef](#)]
45. Majumder, S.; Kono, M.; Lee, Y.T.; Byrnes, C.; Li, C.; Tuymetova, G.; Proia, R.L. A genome-wide CRISPR/Cas9 screen reveals that the aryl hydrocarbon receptor stimulates sphingolipid levels. *J. Biol. Chem.* **2020**, *295*, 4341–4349. [[CrossRef](#)] [[PubMed](#)]
46. Slováčková, J.; Slavík, J.; Kulich, P.; Večeřa, J.; Kováč, O.; Paculová, H.; Straková, N.; Fedr, R.; Silva, J.P.; Carvalho, F.; et al. Polychlorinated environmental toxicants affect sphingolipid metabolism during neurogenesis in vitro. *Toxicology* **2021**, *463*, 152986. [[CrossRef](#)]
47. Liu, Q.; Zhang, L.; Allman, E.L.; Hubbard, T.D.; Murray, I.A.; Hao, F.; Tian, Y.; Gui, W.; Nichols, R.G.; Smith, P.B.; et al. The aryl hydrocarbon receptor activates ceramide biosynthesis in mice contributing to hepatic lipogenesis. *Toxicology* **2021**, *458*, 152831. [[CrossRef](#)]
48. Anitha, M.; Joseph, I.; Ding, X.; Torre, E.R.; Sawchuk, M.A.; Mwangi, S.; Hochman, S.; Sitaraman, S.V.; Anania, F.; Srinivasan, S. Characterization of Fetal and Postnatal Enteric Neuronal Cell Lines with Improvement in Intestinal Neural Function. *Gastroenterology* **2008**, *134*, 1424–1435. [[CrossRef](#)]
49. Pavuk, M.; Schecter, A.J.; Akhtar, F.Z.; E Michalek, J. Serum 2,3,7,8-Tetrachlorodibenzo-p-dioxin (TCDD) Levels and Thyroid Function in Air Force Veterans of the Vietnam War. *Ann. Epidemiol.* **2003**, *13*, 335–343. [[CrossRef](#)]
50. Zhao, B.; DeGroot, D.E.; Hayashi, A.; He, G.; Denison, M.S. CH223191 Is a Ligand-Selective Antagonist of the Ah (Dioxin) Receptor. *Toxicol. Sci.* **2010**, *117*, 393–403. [[CrossRef](#)]
51. Zhu, W.; Wang, X.; Zhou, Y.; Wang, H. C2-Ceramide Induces Cell Death and Protective Autophagy in Head and Neck Squamous Cell Carcinoma Cells. *Int. J. Mol. Sci.* **2014**, *15*, 3336–3355. [[CrossRef](#)] [[PubMed](#)]
52. Zhou, H.; Summers, S.A.; Birnbaum, M.J.; Pittman, R.N. Inhibition of Akt Kinase by Cell-permeable Ceramide and Its Implications for Ceramide-induced Apoptosis. *J. Biol. Chem.* **1998**, *273*, 16568–16575. [[CrossRef](#)] [[PubMed](#)]
53. Summers, S.A.; Garza, L.A.; Zhou, H.; Birnbaum, M.J. Regulation of Insulin-Stimulated Glucose Transporter GLUT4 Translocation and Akt Kinase Activity by Ceramide. *Mol. Cell Biol.* **1998**, *18*, 5457–5464. [[CrossRef](#)] [[PubMed](#)]
54. Mulero-Navarro, S.; Fernandez-Salguero, P.M. New Trends in Aryl Hydrocarbon Receptor Biology. *Front. Cell Dev. Biol.* **2016**, *4*, 45. [[CrossRef](#)] [[PubMed](#)]
55. Sánchez-Martín, F.J.; Fernández-Salguero, P.M.; Merino, J.M. 2,3,7,8-Tetrachlorodibenzo-p-dioxin induces apoptosis in neural growth factor (NGF)-differentiated pheochromocytoma PC12 cells. *NeuroToxicology* **2010**, *31*, 267–276. [[CrossRef](#)] [[PubMed](#)]
56. Sánchez-Martín, F.J.; Fernández-Salguero, P.M.; Merino, J.M. Aryl hydrocarbon receptor-dependent induction of apoptosis by 2,3,7,8-tetrachlorodibenzo-p-dioxin in cerebellar granule cells from mouse. *J. Neurochem.* **2011**, *118*, 153–162. [[CrossRef](#)] [[PubMed](#)]
57. Hill, A.; Howard, C.V.; Strahle, U.; Cossins, A. Neurodevelopmental Defects in Zebrafish (*Danio rerio*) at Environmentally Relevant Dioxin (TCDD) Concentrations. *Toxicol. Sci.* **2003**, *76*, 392–399. [[CrossRef](#)] [[PubMed](#)]
58. Yamaguchi, M.; Hankinson, O. 2,3,7,8-Tetrachlorodibenzo-p-dioxin suppresses the growth of human liver cancer HepG2 cells in vitro: Involvement of cell signaling factors. *Int. J. Oncol.* **2018**, *53*, 1657–1666. [[CrossRef](#)]

59. Chopra, M.; Schrenk, D. Dioxin toxicity, aryl hydrocarbon receptor signaling, and apoptosis—Persistent pollutants affect programmed cell death. *Crit. Rev. Toxicol.* **2011**, *41*, 292–320. [[CrossRef](#)]
60. Heimler, I.; Trewin, A.L.; Chaffin, C.L.; Rawlins, R.G.; Hutz, R.J. Modulation of ovarian follicle maturation and effects on apoptotic cell death in Holtzman rats exposed to 2,3,7,8-tetrachlorodibenzo-p-dioxin (TCDD) in utero and lactationally. *Reprod. Toxicol.* **1998**, *12*, 69–73. [[CrossRef](#)]
61. Jin, M.; Lou, J.; Yu, H.; Miao, M.; Wang, G.; Ai, H.; Huang, Y.; Han, S.; Han, D.; Yu, G. Exposure to 2,3,7,8-tetrachlorodibenzo-p-dioxin promotes inflammation in mouse testes: The critical role of Klotho in Sertoli cells. *Toxicol. Lett.* **2018**, *295*, 134–143. [[CrossRef](#)] [[PubMed](#)]
62. Tian, X.-S.; Xu, H.; He, X.-J.; Li, Y.; He, B.; Zhao, D. Endoplasmic reticulum stress mediates cortical neuron apoptosis after experimental subarachnoid hemorrhage in rats. *Int. J. Clin. Exp. Pathol.* **2020**, *13*, 1569–1577. [[PubMed](#)]
63. Breckenridge, D.G.; Germain, M.; Mathai, J.P.; Nguyen, M.; Shore, G.C. Regulation of apoptosis by endoplasmic reticulum pathways. *Oncogene* **2003**, *22*, 8608–8618. [[CrossRef](#)] [[PubMed](#)]
64. Rao, R.V.; Ellerby, H.M.; E Bredesen, D. Coupling endoplasmic reticulum stress to the cell death program. *Cell Death Differ.* **2004**, *11*, 372–380. [[CrossRef](#)] [[PubMed](#)]
65. Duan, Z.; Zhao, J.; Fan, X.; Tang, C.; Liang, L.; Nie, X.; Liu, J.; Wu, Q.; Xu, G. The PERK-eIF2 α signaling pathway is involved in TCDD-induced ER stress in PC12 cells. *Neurotoxicology* **2014**, *44*, 149–159. [[CrossRef](#)] [[PubMed](#)]
66. Haimovitz-Friedman, A.; Kolesnick, R.N.; Fuks, Z. Ceramide signaling in apoptosis. *Br. Med. Bull.* **1997**, *53*, 539–553. [[CrossRef](#)] [[PubMed](#)]
67. Schwarz, A.; Futerman, A.H. Distinct Roles for Ceramide and Glucosylceramide at Different Stages of Neuronal Growth. *J. Neurosci.* **1997**, *17*, 2929–2938. [[CrossRef](#)] [[PubMed](#)]
68. Brann, A.B.; Scott, R.; Neuberger, Y.; Abulafia, D.; Boldin, S.; Fainzilber, M.; Futerman, A.H. Ceramide Signaling Downstream of the p75 Neurotrophin Receptor Mediates the Effects of Nerve Growth Factor on Outgrowth of Cultured Hippocampal Neurons. *J. Neurosci.* **1999**, *19*, 8199–8206. [[CrossRef](#)] [[PubMed](#)]
69. Siskind, L.J. Mitochondrial Ceramide and the Induction of Apoptosis. *J. Bioenerg. Biomembr.* **2005**, *37*, 143–153. [[CrossRef](#)]
70. Ravid, T.; Tsaba, A.; Gee, P.; Rasooly, R.; Medina, E.A.; Goldkorn, T. Ceramide accumulation precedes caspase-3 activation during apoptosis of A549 human lung adenocarcinoma cells. *Am. J. Physiol. Cell Mol. Physiol.* **2003**, *284*, L1082–L1092. [[CrossRef](#)]
71. Lièvreumont, J.-P.; Sciorati, C.; Morandi, E.; Paolucci, C.; Bunone, G.; Della Valle, G.; Meldolesi, J.; Clementi, E. The p75NTR-induced Apoptotic Program Develops through a Ceramide-Caspase Pathway Negatively Regulated by Nitric Oxide. *J. Biol. Chem.* **1999**, *274*, 15466–15472. [[CrossRef](#)] [[PubMed](#)]
72. Basu, S.; Kolesnick, R. Stress signals for apoptosis: Ceramide and c-Jun kinase. *Oncogene* **1998**, *17*, 3277–3285. [[CrossRef](#)]
73. Hartfield, P.J.; Bilney, A.J.; Murray, A.W. Neurotrophic Factors Prevent Ceramide-Induced Apoptosis Downstream of c-Jun N-Terminal Kinase Activation in PC12 Cells. *J. Neurochem.* **1998**, *71*, 161–169. [[CrossRef](#)] [[PubMed](#)]
74. Gault, C.R.; Obeid, L.M.; Hannun, Y.A. An Overview of Sphingolipid Metabolism: From Synthesis to Break-down. In *Sphingolipids as Signaling and Regulatory Molecules*; Chalfant, C., Poeta, M.D., Eds.; Advances in Experimental Medicine and Biology; Springer New York: New York, NY, USA, 2010; Volume 688, pp. 1–23. ISBN 978-1-4419-6740-4.
75. Jaffrezou, J.-P.; Maestre, N.; de Mas-Mansat, V.; Bezombes, C.; Levade, T.; Laurent, G. Positive feedback control of neutral sphingomyelinase activity by ceramide. *FASEB J.* **1998**, *12*, 999–1006. [[CrossRef](#)] [[PubMed](#)]
76. France-Lanord, V.; Brugg, B.; Michel, P.P.; Agid, Y.; Ruberg, M. Mitochondrial Free Radical Signal in Ceramide-Dependent Apoptosis: A Putative Mechanism for Neuronal Death in Parkinson's Disease. *J. Neurochem.* **1997**, *69*, 1612–1621. [[CrossRef](#)] [[PubMed](#)]
77. Hannun, Y.A. Functions of Ceramide in Coordinating Cellular Responses to Stress. *Science* **1996**, *274*, 1855–1859. [[CrossRef](#)] [[PubMed](#)]
78. Bieberich, E. Ceramide signaling in cancer and stem cells. *Futur. Lipidol.* **2008**, *3*, 273–300. [[CrossRef](#)] [[PubMed](#)]
79. Datta, S.R.; Brunet, A.; Greenberg, M.E. Cellular survival: A play in three Acts. *Genes Dev.* **1999**, *13*, 2905–2927. [[CrossRef](#)] [[PubMed](#)]
80. Rodgers, E.E.; Theibert, A.B. Functions of PI 3-kinase in development of the nervous system. *Int. J. Dev. Neurosci.* **2002**, *20*, 187–197. [[CrossRef](#)]
81. Jacobs, K.M.; Bhave, S.R.; Ferraro, D.J.; Jaboin, J.J.; Hallahan, D.E.; Thotala, D. GSK-3: A Bifunctional Role in Cell Death Pathways. *Int. J. Cell Biol.* **2012**, *2012*, 930710. [[CrossRef](#)]
82. Romorini, L.; Garate, X.; Neiman, G.; Luzzani, C.; Furmento, V.A.; Guberman, A.S.; Sevlever, G.E.; Scassa, M.E.; Miriuka, S.G. AKT/GSK3 β signaling pathway is critically involved in human pluripotent stem cell survival. *Sci. Rep.* **2016**, *6*, 35660. [[CrossRef](#)] [[PubMed](#)]
83. Papadopoli, D.; Pollak, M.; Topisirovic, I. The role of GSK3 in metabolic pathway perturbations in cancer. *Biochim. Biophys. Acta. Mol. Cell Res.* **2021**, *1868*, 119059. [[CrossRef](#)] [[PubMed](#)]
84. Zundel, W.; Giaccia, A. Inhibition of the anti-apoptotic PI(3)K/Akt/Bad pathway by stress. *Genes Dev.* **1998**, *12*, 1941–1946. [[CrossRef](#)] [[PubMed](#)]
85. Heuckeroth, R.O.; Lampe, P.A.; Johnson, E.M.; Milbrandt, J. Neurturin and GDNF Promote Proliferation and Survival of Enteric Neuron and Glial Progenitors in Vitro. *Dev. Biol.* **1998**, *200*, 116–129. [[CrossRef](#)] [[PubMed](#)]

86. Smith, T.H.; Ngwainmbi, J.; Grider, J.R.; Dewey, W.L.; Akbarali, H.I. An In-vitro Preparation of Isolated Enteric Neurons and Glia from the Myenteric Plexus of the Adult Mouse. *J. Vis. Exp.* **2013**, e50688. [[CrossRef](#)]
87. Zhang, Y.; Hu, W. Mouse Enteric Neuronal Cell Culture. In *Neuronal Cell Culture*; Amini, S., White, M.K., Eds.; Methods in Molecular Biology; Humana Press: Totowa, NJ, USA, 2013; Volume 1078, pp. 55–63. ISBN 978-1-62703-639-9.
88. Tian, Y.; Gui, W.; Rimal, B.; Koo, I.; Smith, P.B.; Nichols, R.G.; Cai, J.; Liu, Q.; Patterson, A.D. Metabolic impact of persistent organic pollutants on gut microbiota. *Gut Microbes* **2020**, *12*, 1848209. [[CrossRef](#)]
89. Tsugawa, H.; Cajka, T.; Kind, T.; Ma, Y.; Higgins, B.; Ikeda, K.; Kanazawa, M.; VanderGheynst, J.; Fiehn, O.; Arita, M. MS-DIAL: Data-independent MS/MS deconvolution for comprehensive metabolome analysis. *Nat. Methods* **2015**, *12*, 523–526. [[CrossRef](#)]

Disclaimer/Publisher’s Note: The statements, opinions and data contained in all publications are solely those of the individual author(s) and contributor(s) and not of MDPI and/or the editor(s). MDPI and/or the editor(s) disclaim responsibility for any injury to people or property resulting from any ideas, methods, instructions or products referred to in the content.